Thermal fluctuations and phase equilibrium in microemulsions

Leonardo Golubović
Department of Physics and the Solid State Center, University of California, Los Angeles, Los Angeles, California 90024

T. C. Lubensky
Department of Physics, University of Pennsylvania, Philadelphia, Pennsylvania 19104-6396

(Received 13 June 1989)

We construct a simple coarse-grained model and use it to study global phase behavior of ensembles of fluid membranes. This model is an improvement over previous phenomenological models of Talmon and Prager, de Gennes and co-workers, Widom, and more recently of Safran and coworkers. We show here that there is necessarily an entropic contribution, missing in all previous theories, to the coarse-grained free energy whose physical origin is the same as that of Helfrich's entropic repulsion stabilizing lamellar multimembrane phases. The inclusion of this steric entropy in the previous phenomenological studies is essential if they are to be used in the study of periodic phases in microemulsions and analogous surfactant systems. Thus the model enables us to obtain, in a unified way, phase diagrams containing both uniform and periodic phases in microemulsions and in binary systems of nonionic surfactant bilayers in a single solvent. Mean-field theory for this model yields rich phase diagrams containing dilute, random bicontinuous, lamellar, columnar, and an antiferromagnetic phase that may correspond to a droplet crystal or to a "plumber's nightmare." The model depends on two phenomenological parameters related to strengths of steric entropy and softening of membrane rigidity. We discuss the sensitivity of phase diagrams (in particular the existence of the middle-phase microemulsion) to values of these parameters. We find that the existence of a realistic middle phase (with structural length scale much larger than the molecular length scale) crucially depends on the presence of steric entropy. The model reproduces the experimentally observed four-phase equilibria among uniform phases in microemulsions.

I. INTRODUCTION

A. Phenomenological approach to ensembles of fluid membranes

In recent years there has been considerable progress[1-4] in understanding the phase behavior of microemulsions and related complex fluids involving surfactants. Surfactant molecules in these systems typically form extensive surfaces with fluid internal order. In the case of microemulsions these surfaces are flexible fluid monolayer membranes that form at interfaces between oil and water because of the amphiphilic nature of surfactant molecules.[5,6] In some binary mixtures of surfactant and a single solvent, phases of bilayer surfactant sheets similar to those occurring in microemulsions have been found to occur at surfactant volume fractions of a few percent.[7]

The phase diagrams of these systems are remarkably rich. In microemulsions, when the volume factions of oil and water are comparable, a random bicontinuous isotropic phase consisting of percolating domains of water and oil may arise.[5] Under appropriate conditions (e.g., for volume fractions of surfactant higher than a few percent) various periodic—lamellar, cubic, or columnar—structures occur.[8] Finally, at very small surfactant volume fraction, phase separation into dilute phases of oil with a small amount of water and vice versa occurs (see Fig. 1).

It is currently believed that this rich phase behavior can be explained in terms of the thermodynamics of an ensemble of self-avoiding thermally fluctuating incompressible fluid membranes.[1-4] For example, the coexistence of dilute and random bicontinuous phases in microemulsions [Fig. 1(d)] has been explained by Safran *et al.*[1] by a phenomenological theory of such an ensemble.[9] The essence of this theory is a coarse-graining of interfacial fluctuations: the space occupied by the microemulsion is divided into a simple-cubic lattice of cells of side ξ; each cell is filled with water or oil, while surfactant molecules are presumed to form incompressible fluid monolayers at oil-water interfaces. A random mixing approximation is used to account for the entropy of interfaces at length scales larger than ξ. Fluctuations at shorter length scales are taken into account by allowing the bending elastic constant $K(\xi)$ for interfaces to depend on the length scale ξ.[10-12] When ξ is of order ξ_p, the de Gennes–Taupin persistence length,[13] $K(\xi)$ is typically of order $k_B T$. This model successfully predicts dilute-bicontinuous phase coexistence with the structural length scale ξ of order ξ_p in the random bicontinuous phase (in this case called the middle phase).

To date, the above phenomenological approach has been consistently applied only to the study of phase equilibria between spatially uniform phases which occur in microemulsion systems (dilute and random bicontinuous phases[1]) or in systems of bilayer fluid membranes dissolved in a single solvent [dilute (micellar) and sheetlike

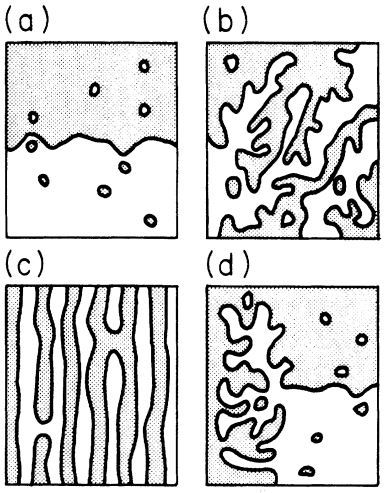

FIG. 1. (a) Dilute phases consisting of oil droplets in a water background and vice versa. The oil-rich phase is indicated with dots. Dilute phases occur at low ϕ_s (say, less than 1%) and are the analog of positive and negative magnetization ordered phases of the Ising model. (b) The random bicontinuous phase of percolating oil and water domains. This phase occurs at ϕ_s of the order of a few percent and is the analog of the paramagnetic phase of the Ising model. (c) The lamellar phase consisting of alternating layers of water and oil. This phase occurs at ϕ_s greater than a few percent. This figure shows defects in the form of water passages through an oil layer and vice versa. (d) Three-phase coexistence of the two dilute phases and the random bicontinuous phase. When there is such three-phase coexistence, the random bicontinuous phase is called the middle phase.

isotropic phases[2]]. Phase equilibria between uniform phases and the nearby sterically stabilized lamellar phase were also studied in Refs. 1 and 2. However, as noted by the authors, the lamellar and uniform phases were not treated in a unified way. The free energy of uniform phases was calculated using the phenomenological theory and compared with the free energy of the perfectly ordered lamellar phase [i.e., one without defects such as those in Fig. 1(c) disrupting translational order of the phase] as estimated from the Helfrich's expression for the steric free energy of self-avoiding undulating membranes comprising the lamellar phase.[14] In this paper, our main goal is to develop a theory which treats in a unified way transitions between various phases, both uniform and nonuniform (lamellar, columnar, cubic, etc.), occurring in ensembles of fluctuating fluid membranes.

B. Steric entropy and nonuniform phases

In this section we outline our approach to the construction of a phenomenological theory of phase equilibria in microemulsions and related ensembles of fluid membranes. For concreteness, we will speak in terms appropriate to microemulsions. We stress, however, that applications of this theory to related problems, e.g., systems of bilayers in a single solvent [2], are straightforward.

As in previous phenomenological studies,[1-3,9] our coarse-graining procedure is implemented by dividing space into a simple-cubic lattice of cells of side ξ. With each cell i we associate an Ising spin variable ϕ_i which satisfies $\phi_i=0$ if the center of the cell is occupied by water and $\phi_i=1$ if it is occupied by oil [see Figs. 2(a) and 2(b)]. For a given configuration of spins $\{\phi_i\}$, one can construct a set of smooth mean interfaces $\{S_j\}$ between oil and water domains [see Fig. 2(b)], and describe them, as in the approach of Safran *et al.*,[1-3] in terms of length- (i.e., ξ) dependent elastic constants. These differ from bare constants because coarse-graining [i.e., the passage from the situation in Fig. 2(a) to that in Fig. 2(b)] involves integrating some short-scale interface fluctuations out of the random surface partition function. The geometry of the mean smooth interfaces $\{S_j\}$ is determined by the spin configuration $\{\phi_i\}$ [see Fig. 2(b)]. Then, knowing the effective elastic constants of mean interfaces, one can associate a coarse-grained spin Hamiltonian $H(\{\phi_i\})$ to a given $\{\phi\}$. This Hamiltonian is the sum of free energies of individual smooth interfaces:

$$H(\{\phi_i\})=\sum_j f_j \ , \tag{1.1}$$

where f_j is the free energy of the jth smooth interface S_j in Fig. 2(b).

The idea behind the construction of $H(\{\phi_i\})$ is basically the same as that embedded in the coarse-graining in standard renormalization-group theories: an effective action for long-length-scale fluctuations arises from decima-

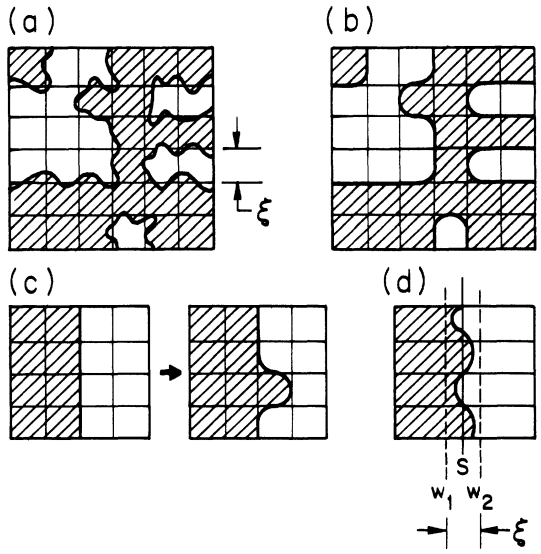

FIG. 2. Coarse graining of membrane fluctuations is implemented by dividing space into cubic cells of side ξ and replacing the rapidly fluctuating interfaces shown in (a) by smooth mean interfaces shown in (b). The smooth interfaces are characterized by effective elastic constants. (c) A large fluctuation changing one configuration of cell spins into another. (d) In order to avoid large fluctuations such as shown in (c), a hard wall constraint is imposed, limiting short-scale fluctuations, which are integrated out of the surface partition function. Oil regions are hatched.

tion of short-scale fluctuations. In our case large, long-length-scale interfacial fluctuations are those converting one spin configuration $\{\phi_i\}$ into another $\{\phi_i'\}$ [see Fig. 2(c)]—the coarse-grained Hamiltonian $H(\{\phi_i\})$ of Eq. (1.1) describes the statistics of these fluctuations. On the other hand, in order to avoid overcounting of configurations, short-scale interfacial fluctuations, which we plan to decimate, are not allowed to change one spin configuration into another. In practice, this means that the short-scale height fluctuations normal to smooth mean interfaces $\{S_j\}$ are constrained to be less than some length which is of order of the cell size ξ as depicted in Fig. 2(d). To implement this constraint on short-scale interfacial fluctuations, we surround each S_j with two hard walls w_j^1 and w_j^2 at respective normal distance $\xi/2$ and $-\xi/2$ from S_j. These walls constrain short-scale interfacial fluctuations so that they do not change the configuration of occupation numbers $\{\phi_i\}$ [as they would in the absence of walls as can be seen by comparing Figs. 2(c) and 2(d)].

These observations lead us to the following recipe for constructing the effective spin Hamiltonian $H(\{\phi_i\})$: A given configuration of spins $\{\phi_i\}$ defines a set of smooth interfaces $\{S_j\}$. [It may happen that more than just one set $\{S_j\}$ can be associated with a given $\{\phi_i\}$ as depicted in Figs. 3(b) and 3(c). For the moment, let us presume that $\{S_j\}$ is uniquely determined by a given $\{\phi_i\}$, as in Figs. 2(a) and 2(b).] Each S_j can be thought of as the mean surface drawn between two hard walls, w_j^1 and w_j^2, a distance ξ apart as depicted in Figs. 2(d) and 3(b) and 3(c). Fluctuations of the jth interface around the mean

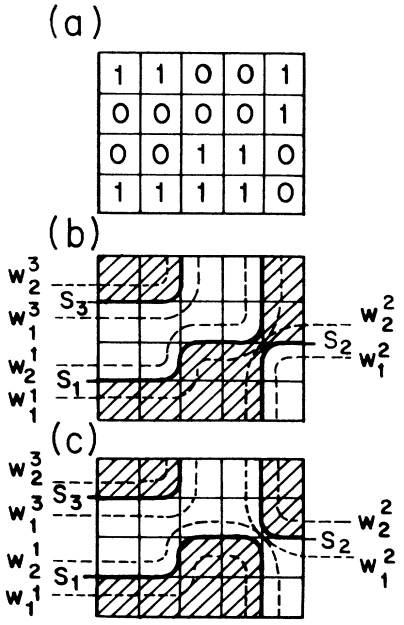

FIG. 3. A given configuration of cell spins $\{\phi_i\}$ defines at least one set of smooth mean interfaces $\{S_j\}$. Thus the set of occupation numbers $\{\phi_i\}$ in (a) defines the two sets of surfaces $\{S_j\}$ shown in (b) and (c). Two hard walls w_j^1 and w_j^2 are placed around each S_j in order to suppress large fluctuations which may alter the cell spin configuration in (a). Oil regions are hatched.

interface S_j, constrained to lie between w_j^1 and w_j^2, do not change the occupation number configuration $\{\phi_j\}$. These fluctuations are indeed the short-length-scale fluctuations we wish to integrate out of the surface partition function in order to obtain the effective spin Hamiltonian, Eq. (1.1). $H(\{\phi_j\})$ is the free energy of these fluctuations. Each entry f_j in the sum (1.1) is the free energy of the interface confined between walls w_j^1 and w_j^2. The calculation of f_j is by itself an entirely nontrivial problem of statistical mechanics. It can be done approximately when S_j is a planar or nearly planar surface (see Sec. II B and Ref. 15). The final expression for f_j (see Sec. II B) contains a part expressed in terms of renormalized elastic constants similar to that of Refs. 1–3. In addition to this, it contains an entropic contribution, missing in all previous phenomenological studies,[1–3,9] whose origin is the same as that of the Helfrich entropic repulsion[14] stabilizing lamellar multimembrane phases.[16] This contribution to f_j arises from the difference in entropy of a free interface and one which is confined by hard walls. Because we interpret short-scale fluctuations as fluctuations of surfaces confined by hard walls,[15,17] this *steric entropy* naturally enters our coarse-grained Hamiltonian (1.1). The presence of walls reduces wandering entropy of otherwise rough interfaces, yielding a positive free-energy contribution[18] to f_j, i.e., to the effective Hamiltonian (1.1).

Having constructed $H(\{\phi_i\})$, one may proceed to study fluctuations of $\{\phi_i\}$, as well as to determine the phase diagram of the system. We accomplish this approximately by mean-field theory as detailed in Secs. III and IV. The resulting phase diagrams contain both uniform and nonuniform, i.e., periodic phases. Uniform phases correspond to states which have i-independent average occupation numbers $\langle\phi_i\rangle$ and include the random bicontinuous phase ($\langle\phi_i\rangle=\frac{1}{2}$) and dilute phases ($\langle\phi_i\rangle\neq\frac{1}{2}$). The bicontinuous [Fig. 1(b)] and dilute [Fig. 1(a)] phases correspond, respectively, to the paramagnetic and ferromagnetic phases of the model with a spatially uniform, i.e., i-independent order parameter, $\langle\phi_i\rangle-\frac{1}{2}$. Periodic phases are characterized by a spatially varying, i.e., by an i-dependent order parameter, $\langle\phi_i\rangle-\frac{1}{2}$. Thus, the lamellar phase is a layered state with block cells partitioned into alternating even and odd layers of thickness ξ [see Fig. 4(a)] corresponding, respectively, to oil and water layers of the lamellar microemulsion. For each site i belonging to an even layer,

$$\langle\phi_i\rangle=\phi\ , \tag{1.2a}$$

while for each i belonging to an odd layer,

$$\langle\phi_i\rangle=1-\phi\ . \tag{1.2b}$$

The perfectly ordered lamellar structure [Fig. 5(a)] corresponds to a state with $\phi=1$ or $\phi=0$ in Eqs. (1.2). (The state with $\phi=0$ can be converted to that with $\phi=1$ via a uniform translation normal to the lamellae.) When $\frac{1}{2}<\phi<1$ there are defects in the lamellae, e.g., passages of water through oil layers or of oil through water as shown in Fig. 5(b). Finally, when $\phi=\frac{1}{2}$ in Eq. (1.2), the average cell occupation number is spatially uniform, and

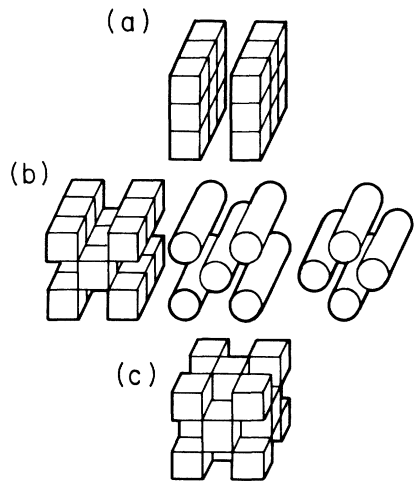

FIG. 4. (a) Cell spin representation of the perfectly ordered lamellar phase. Only oil cubes are represented. (b) The same for the columnar phase. Smoothing of sharp edges yields two kinds of columnar phases coexisting at zero spontaneous curvature—columns of oil in water and vice versa. (c) Antiferromagnetic phase corresponding to a droplet crystal.

the state of the system is that of the random bicontinuous microemulsion. Our approach allows us to study the nature of the phase transition between the lamellar and bicontinuous phases (see Sec. IV), whether it is second order (ϕ goes continuously to $\frac{1}{2}$ upon changing a parameter of the system) or first order (ϕ jumps discontinuously from $\phi > \frac{1}{2}$ to $\phi = \frac{1}{2}$).

Nonuniform phases other than the lamellar phase appear in a similar fashion. Thus, the columnar phase corresponds to two-dimensional ordering of alternating oil and water columns of block cells [Fig. 4(b)]. Oil columns are, once again, characterized by Eq. (1.2a), water columns by (1.2b). This columnar phase corresponds in microemulsions to two coexisting tubular phases [see Fig. 4(b) and Secs. II and III for details]. Another periodic phase we find is one with cubic symmetry arising from a three-dimensional antiferromagnetic ordering of cell spins [Fig. 4(c)] with $\langle \phi_i \rangle = \langle \phi_j \rangle$ if sites i and j are next-nearest neighbors and $\langle \phi_i \rangle = 1 - \langle \phi_j \rangle$ if sites i and j are nearest neighbors. Thus, the lattice is once again partitioned into oil sites, satisfying Eq. (1.2a), and water sites, satisfying Eq. (1.2b). This antiferromagnetic phase of the lattice model may correspond in microemulsions to an fcc droplet crystal (see Secs. II and III) or possibly to some kind of "plumber's nightmare" (see Sec. V). In Sec. IV we find that this phase may strongly compete with the lamellar phase.

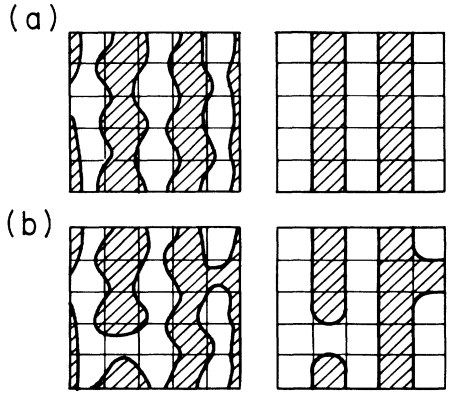

FIG. 5. (a) A configuration in a perfectly ordered lamellar phase and its coarse-grained configuration. (b) The same for a lamellar phase with defects. Oil regions are hatched.

In this paper we study transitions between the phases described above. Our study is based upon an approximate coarse-grained Hamiltonian $H(\{\phi_i\})$ derived in Sec. II along the lines indicated above. In applications to uniform phases, this Hamiltonian leads to results which are essentially those of Safran *et al.*[1] (we present a somewhat more detailed discussion of the influence of some phenomenological parameters on the phase diagram, e.g., on the existence of the middle phase microemulsion). We, however, introduce order parameters, reducing to zero in the spatially uniform random bicontinuous phase, that describe order in spatially nonuniform phases. We are, therefore, able to calculate phase diagrams with spatially nonuniform phases from a single phenomenological Hamiltonian. An important improvement of our approach relative to previous studies is the incorporation of Helfrich's steric entropy into the coarse-grained lattice Hamiltonian which serves as the basis for our phenomenological study. This is the crucial ingredient that allows us to treat the lamellar phase, which is stabilized by steric entropy. The contribution to our coarse-grained Hamiltonian from steric entropy arises naturally in our treatment as a result of the removal of short-scale fluctuations.

It should be stressed that our approach shares many deficiencies of previous phenomenological studies. For example, polydispersivity is ignored (we consider only a single length scale ξ, which is variationally determined as discussed in Secs. II and III). The effects of Gaussian curvature are not included, and our use of some regular lattice produces an artificial spatial anisotropy not present in microemulsions. Finally, we limit ourselves to studying fluctuations at length scales longer than ξ by a mean-field approach. These matters are discussed throughout this paper and particularly in Sec. V.

The layout of the paper is as follows: in Sec. II we discuss thermodynamic ensembles of fluctuating fluid membranes and construct the coarse-grained lattice Hamiltonian. The derivation of mean-field theory is given in Sec. III. In Sec. IV we present phase diagrams of microemulsions obtained from the mean-field theory and comparisons with experiments (Sec. IV C). A summary and discussion are presented in Sec. V, while some details relevant for Sec. II B are presented in the Appendix.

II. COARSE GRAINING AND THE LATTICE MODEL

A. Thermodynamic ensembles of fluid membranes

Let us consider the thermodynamics of a ternary, oil-water-surfactant mixture with total volume $V = V_o' + V_w'$

$+V_s$, where V_o', V_w', and V_s are, respectively, the volumes occupied by oil, water, and surfactant. As in previous phenomenological studies[1-3] we presume that oil and water are incompressible and that the entire amount of the surfactant is absorbed at interfaces between oil and water regions forming incompressible fluid monolayers of thickness w and of total area A. Thus, the volume fraction of surfactant is

$$\phi_s = \frac{V_s}{V} = \frac{Aw}{V} , \tag{2.1}$$

which is typically of order of a few percent in microemulsion systems. To describe the thermodynamics of such a system, we envision it as a collection of oriented surfaces and define $V_o = V_o' + V_s/2$ and $V_w = V_w' + V_s/2$ as, respectively, the total volume of the system on oil and water sides of these surfaces. Surfaces are allowed to merge or divide into smaller ones—thus the total number of membranes is variable. However, since the total volume of surfactant or, by Eq. (2.1), the total area A of interfaces is fixed, one has to impose the constraint

$$A = \sum_j A(\mathbf{R}_j) \tag{2.2}$$

on the ensemble of fluid membranes. $A(\mathbf{R}_j)$ in Eq. (2.2) is the area of the jth surface, which is a functional of a three-dimensional vector field $\mathbf{R}_j$ specifying positions of the surface points,[19] given simply by

$$A(\mathbf{R}_j) = \int d^2 s_j . \tag{2.3}$$

Surfaces in microemulsion systems are interfaces between oil and water regions and are, therefore, as anticipated in Sec. I, the exact analog of interfaces separating up and down spin regions in an Ising system. Thus, they are closed, self-avoiding, oriented (say, from water to oil) surfaces. For a given configuration of surfaces $\{\mathbf{R}_j\}$, let us define the functional $W(\{\mathbf{R}_j\})$ to represent the total volume of the system on the oil side of surfaces (corresponding, after coarse-graining, to the total number of oil sites with $\phi_i = 1$ as discussed in Sec. I). Since both oil and water are considered to be incompressible, one has to impose the constraint

$$V_o = W(\{\mathbf{R}_j\}) \tag{2.4}$$

on the ensemble of fluid membranes.

The partition function associated with the ensemble constrained by Eqs. (2.2) and (2.4) must be a sum over a variable number of surfaces. Terms of this sum which correspond to a sector with some fixed number of surfaces are sums over all possible topologies (number of handles) for each surface,[19] as well as, for a given topology, integrals over all possible shapes of surfaces.[20] Let us denote the trace operator performing this summation over states with a variable number of surfaces, having variable topologies and shapes, by $\mathrm{Tr}_{\{\mathbf{R}_j\}}$. This operator as well as a Boltzmann factor of the partition function have to be reparametrization invariant.[12,15,19,20] The Boltzmann factor must ensure self-avoidance of surfaces,[21] as well as reflect bending elasticity of fluid membranes.[22] It is of the form $\exp[-H(\{\mathbf{R}_j\})/T]$ (in units with $k_B = 1$) with

$$H(\{\mathbf{R}_j\}) = \sum_j H_B(\mathbf{R}_j) + H_{\mathrm{SAW}}(\{\mathbf{R}_j\}) . \tag{2.5}$$

H_{SAW} in (2.5) is the strict, hard-core self-avoidance interaction, while $H_B(\mathbf{R}_j)$ is the bending elastic Hamiltonian, which is a functional of the principal radii of curvature r_1 and r_2. To the lowest order in r_1^{-1} and r_2^{-1} this Hamiltonian reads[22]

$$H_B(\mathbf{R}_j) = \int d^2 s_j \left[\frac{1}{2} K_M \left(\frac{1}{r_1} + \frac{1}{r_2} - \frac{2}{r_0} \right)^2 + K_G \frac{1}{r_1 r_2} \right] . \tag{2.6}$$

The elastic constants K_M and K_G determine, respectively, the bending elastic energy due to nonzero mean, $(r_1^{-1} + r_2^{-1})$, and Gaussian, $(r_1 r_2)^{-1}$, curvatures.[19] r_0 in Eq. (2.6) is the so-called spontaneous radius of curvature. It reflects the tendency of realistic membranes to bend spontaneously either toward the oil ($r_0^{-1} > 0$) or toward the water ($r_0^{-1} < 0$) side of surfaces. Throughout the paper we will be mainly interested in the so-called balanced systems with $r_0^{-1} = 0$. We note that reduced rigidity constants K_M/T and K_G/T are dimensionless. The bending energy arising from the Gaussian curvature term is a topological invariant of a closed surface:[19] regardless of the surface's shape, it is determined by the surface topology via the formula $4\pi(1-h)K_G$, with h, the number of handles (e.g., $h = 1$ for toruslike surfaces, $h = 0$ for surfaces isomorphic to sphere). Positive K_G thus favors, for example, fusion of two droplets into a single one, or a creation of an oil passage through a water layer in lamellar microemulsions—in both cases the energy gained due to Gaussian curvature[23] is $4\pi K_G$ (see Fig. 6).

The free energy density, respecting constraints (2.2) and (2.4), is

$$G\left(\frac{A}{V}, \frac{V_o}{V} \right) = -\frac{T}{V} \ln \left[\mathrm{Tr}_{\{\mathbf{R}_j\}} \delta \left(A - \sum_j A(\mathbf{R}_j) \right) \times \delta(V_o - W(\{\mathbf{R}_j\})) e^{-H(\{\mathbf{R}_j\})/T} \right] . \tag{2.7}$$

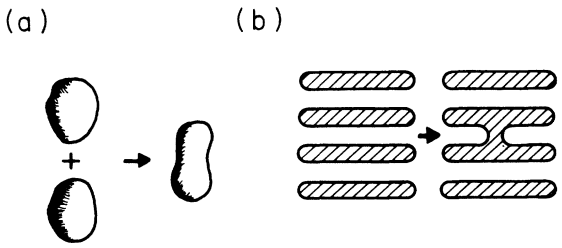

FIG. 6. Positive Gaussian curvature bending constant K_G favors fusion of the droplets in (a) as well as the creation of the passage in the lamellar phase in (b). In both cases the topologically invariant part of the bending energy decreases by $4\pi K_G$.

It is convenient to introduce the unconstrained free energy density $F(\sigma,\mu_o)$ by

$$F(\sigma,\mu_o) = -\frac{T}{V}\ln\left\{\mathrm{Tr}_{\{\mathbf{R}_j\}}\exp\left[-\frac{1}{T}\left[H(\{\mathbf{R}_j\})+\sigma\sum_j A(\mathbf{R}_j) - \mu_o W(\{\mathbf{R}_j\})\right]\right]\right\} \tag{2.8}$$

defined in terms of two chemical potentials: σ, the bare surface tension, coupled to total surface area, and μ_o, the chemical potential coupled to the volume of the system on the oil side of interfaces.[24] In the thermodynamic limit, $V\to\infty$, $V_o\to\infty$, $A\to\infty$, with A/V and V_o/V fixed, the free-energy densities G, Eq. (2.7), and F, Eq. (2.8), are related by the Legendre transform

$$G\left[\frac{A}{V},\frac{V_o}{V}\right] = \left[-\sigma\frac{A}{V}+\mu_o\frac{V_o}{V}+F(\sigma,\mu_o)\right]_{\mathrm{var}(\sigma,\mu_o)}, \tag{2.9}$$

where $[f(x,y)]_{\mathrm{var}(x,y)}$ denotes the dominant saddle point of $f(x,y)$, so that variation over σ gives

$$\frac{A}{V} = \frac{\partial F}{\partial\sigma}, \tag{2.10}$$

while variation over μ_o gives

$$\frac{V_o}{V} = -\frac{\partial F}{\partial\mu_o}. \tag{2.11}$$

The unconstrained free-energy density $F(\sigma,\mu_o)$ is more fundamental for studying phase equilibrium in microemulsions—at first order phase transitions phases having different volume fractions of surfactant (wA/V) and oil (V_o/V) coexist at the same value of σ and μ_o.[24] In the following we construct an approximate coarse-grained Hamiltonian by starting from the unconstrained partition function (2.8).

B. Coarse-graining of membrane fluctuations

In this section and Sec. II C we proceed to implement the program outlined in Sec. I B, i.e., to construct the effective coarse-grained lattice Hamiltonian $H(\{\phi_i\})$ that is a function of "spins" ϕ_i indicating whether the center of the cell i of volume ξ^3 of a simple-cubic lattice is occupied by water ($\phi_i=0$) or by oil ($\phi_i=1$). Each spin configuration $\{\phi_i\}$ defines a set $\{S_j\}$ of smooth interfaces separating oil and water domains. As explained in Sec. I, coarse-graining consists of integrating out of the unconstrained partition function (2.8) all surface fluctuations that do not change occupation numbers ϕ_i. Thus, the height fluctuations of the jth interface above a smooth mean interface S_j are constrained to be less than some length of order the cell size ξ (Fig. 3). Then, $H(\{\phi_i\})$ is given by Eq. (1.1),

$$H(\{\phi_i\}) = \sum_j f_j, \tag{2.12}$$

with f_j the free energy of a fluid membrane constrained to fluctuate around the mean surface S_j by two hard walls, w_j^1 and w_j^2, separated by a constant distance ξ as depicted in Fig. 7. As observed in Sec. I B, f_j is a functional of the shape of S_j and ultimately can be expressed in terms of the spin configuration $\{\phi_i\}$. Thus, the free-energy density $F(\sigma,\mu_o)$, Eq. (2.8), can be approximated by

$$F(\sigma,\mu_o,\xi) = -\frac{T}{V}\ln\left\{\mathrm{Tr}_{\{\phi_i\}}\exp\left[-\frac{1}{T}\left[H(\{\phi_i\})-\mu_o\sum_i\phi_i\xi^3\right]\right]\right\} \tag{2.13}$$

with $H(\{\phi_i\})$ given by Eq. (2.12).

In (2.13) we replaced the functional $W(\{R_j\})$ figuring in Eq. (2.8) by the volume $\sum_i\phi_i\xi^3$ of oil cells (we recall that short-scale fluctuations are defined as those which do not change the coarse-grained occupation numbers ϕ_i). Furthermore, the sum over the number of surfaces, as well as the sum over topologies entering the trace operator in Eq. (2.8) is replaced in (2.13) by the ordinary sum over all spin configurations

$$\mathrm{Tr}_{\{\phi_i\}} = \prod_i\sum_{\phi_i=0,1}. \tag{2.14}$$

Note that, in contrast to $F(\sigma,\mu_o)$ the free energy (2.13) contains an additional parameter, the cell size ξ. We will argue in the following that $F(\sigma,\mu_o)$ is the minimum of $F(\sigma,\mu_o,\xi)$ with respect to ξ

$$F(\sigma,\mu_o) = [F(\sigma,\mu_o,\xi)]_{\mathrm{var}(\xi)} \tag{2.15}$$

at constant V and σ.

Now we proceed to calculate $H(\{\phi_i\})$ via Eq. (2.12). To accomplish this we need an approximation for f_j, which is, in general, a function of ξ (the distance between imaginary hard walls w_j^1 and w_j^2) and a functional of the vector field $\mathbf{R}_j^0$ which specifies the shape of the mean surface S_j between the walls w_j^1 and w_j^2 (see Fig. 7):

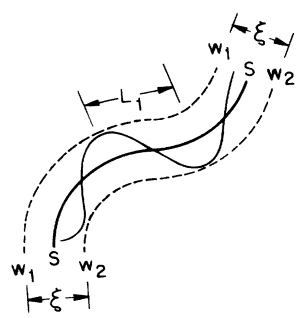

FIG. 7. A membrane constrained to fluctuate around the mean interface S by hard walls w_1 and w_2 at respective normal distances $+\xi/2$ and $-\xi/2$ from S.

$$f_j = f(\xi; \mathbf{R}_j^0) \ . \tag{2.16}$$

An approximate formula for f_j (see Ref. 15 and the Appendix) in the limit where the mean free length L_1 between collisions of the surface with hard walls is much smaller than the principal radii of curvature r_1 and r_2 of the mean surface S_j, is given when there is no spontaneous curvature ($r_0^{-1} = 0$) by

$$f(\xi, \mathbf{R}_j^0) = \int d^2 s_j \left[a(L_1) + \tfrac{1}{2} K_M(L_1) \left(\frac{1}{r_1} + \frac{1}{r_2} \right)^2 + K_G(L_1) \frac{1}{r_1 r_2} \right] . \tag{2.17}$$

We proceed to define entries of (2.17). The integral in (2.17) is over the mean surface S_j . The form of the free energy (2.17) is that of a surface which has an effective surface tension $a(L_1)$ and effective bending constants $K_M(L_1)$ and $K_G(L_1)$. The length L_1 is related to the distance ξ between walls by

$$(\xi - w)^2 = L_1^2 T / [32\pi\mu K_M(L_1)] \tag{2.18}$$

with w the membrane thickness. The constant μ in (2.18) is a dimensionless phenomenological parameter, originally introduced by Helfrich[14] in his theory of smectic elasticity of lamellar multimembrane phases. It is a number of order unity.[15] The choice,

$$\mu = 1/(3\pi^2) \ , \tag{2.19}$$

proposed by Helfrich[14] seems to be in agreement with some experiments on lyotropic lamellar systems.[16] In Sec. IV we will study the sensitivity of the phase diagrams to changing μ in the reasonable range

$$10^{-1} \lesssim \mu \lesssim 1 \ . \tag{2.20}$$

The physical meaning of (2.18) is simple: height fluctuations of a finite free membrane of side L_1 are of order[15,17]

$$l^2 \approx L_1^2 T / K_M(L_1) \ . \tag{2.21}$$

Thus, a large membrane confined between two walls separated by ξ will undergo collisions with the walls, with the average distance between collisions L_1, which satisfies Eq. (2.21) with $l \approx \xi - w$, and Eq. (2.18) follows.

Thus, at length scales larger than L_1, membrane fluctuations are strongly constrained by the presence of the walls. At scales less than L_1, fluctuations are like those of a free membrane in the absence of walls; the major effect of these fluctuations is a strong length-scale dependence of the effective bending constants $K_M(L_1)$ and $K_G(L_1)$ of Eq. (2.17), given by

$$K_M(L_1) = K_M(a) - \frac{\alpha T}{4\pi} \ln \frac{L_1}{a} \equiv \frac{\alpha T}{4\pi} \ln \frac{\xi_p}{L_1} \ , \tag{2.22}$$

$$K_G(L_1) = K_G(a) + \frac{\alpha' T}{4\pi} \ln \frac{L_1}{a} \tag{2.23}$$

with $\alpha = 3$ and $\alpha' = \frac{10}{3}$ (see Refs. 11, 12, and 15; Helfrich[10] recently proposed arguments in favor of $\alpha = 1$, $\alpha' = 0$). As demonstrated in Sec. IV, the details of phase diagrams are strongly dependent on the actual value of α, while independent of α' (as a result of our crude approximation of mean surfaces as a sum of elements which have zero Gaussian curvature). In Eq.(2.22), we introduced the de Gennes–Taupin persistence length:[13]

$$\xi_p = a \exp \left[\frac{4\pi K(a)}{\alpha} \right] . \tag{2.22'}$$

The length a in Eqs. (2.22) to (2.24) is a short-distance cutoff. It is of order of the distance between surfactant molecules in the surface or, possibly, of the membrane thickness w . In the following we will set $a = w$. In fact, by a simple redefinition of the bare parameters $K_M(a)$ and $K_G(a)$ in Eqs. (2.22) and (2.23), one can easily show that this assumption has no effect on the structure of phase diagrams.

Finally, we discuss the surface area term $a(L_1)$ of Eq. (2.17). It has the form[15]

$$a(L_1) = \sigma_R(L_1) + F_{\rm st}, \tag{2.24}$$

with

$$\sigma_R(L_1) = (\sigma - \sigma_0) \left[1 + \frac{1}{4\pi K(a)} \ln \frac{L_1}{a} \right], \tag{2.25}$$

and

$$F_{\rm st} = \frac{\pi T}{4 L_1^2} \ . \tag{2.26}$$

σ_0 in Eq. (2.25) is a constant dependent on the $K_M(a)$ and a (see Ref. 15)—its precise value does not affect the structure of phase diagrams, which can be expressed as a function of a subtracted surface tension,

$$\sigma_s = \sigma - \sigma_0 \ . \tag{2.27}$$

$F_{\rm st}$, Eq. (2.26), is the steric free energy density (per unit area) introduced originally by Helfrich.[14] It is an entropic interaction coming from the fact that each collision of the surface with the walls reduces the membrane entropy (with respect to the one of a free membrane) by an amount of order unity.[18] Thus, the surface free energy increase corresponding to this *steric entropy* is of order T per collision, i.e., of order T/L_1^2 per unit area of the mean surface S_j as described by Eq. (2.26). By means of Eq. (2.18), $F_{\rm st}$ can be rewritten as

$$F_{\rm st} = T^2 / [128\mu(\xi - w)^2 K_M(L_1)]. \tag{2.28}$$

So, to summarize, the coarse-grained Hamiltonian (2.12) can be written, by Eq. (2.17), as

$$H(\{\phi_i\}) = a(L_1) A(\{\phi_i\}) + K_M(L_1) B_M(\{\phi_i\}) + K_G(L_1) B_G(\{\phi_i\}), \tag{2.29}$$

with $a(L_1)$, $K_M(L_1)$, and $K_G(L_1)$ given, respectively, by Eqs. (2.24)–(2.27), (2.22) and (2.23), with L_1 related to ξ by Eq. (2.18). Each of the entries A, B_M, and B_G of (2.29) is given by a sum of the integrals over smooth average interfaces $\{S_j\}$, of the form

$$A(\{\phi_i\}) = \sum_j \int d^2 s_j \ , \tag{2.30}$$

$$B_M(\{\phi_i\})=\sum_j \int d^2s_j \frac{1}{2}\left[\frac{1}{r_1}+\frac{1}{r_2}\right]^2 , \tag{2.31}$$

and

$$B_G(\{\phi_i\})=\sum_j \int d^2s_j \frac{1}{r_1 r_2} . \tag{2.32}$$

A, B_M, and B_G are functionals of the spin configuration $\{\phi_i\}$—positions of smooth average interfaces S_j between water and oil domains are to be determined from the knowledge of occupation numbers ϕ_i (see Sec. II C).

Note that, by Eq. (2.22), when the mean free length L_1 of a membrane is of order but somewhat less than the persistence length ξ_p, one has

$$K_M(\xi_p)\approx T \tag{2.33}$$

and, by (2.18)

$$\xi\approx L_1\approx\xi_p . \tag{2.34}$$

The typical structural length ξ we obtain in the random microemulsion is of order ξ_p in agreement with Safran *et al.*[1] Then, Eqs. (2.33) and (2.34) ensure that the contribution of the steric free energy (2.26) is comparable to those of other interactions of the coarse-grained Hamiltonian (as will become more clear in the following sections). Thus, the inclusion of steric effects is necessary to obtain a complete theory of microemulsion systems.

The typical length scale ξ in the lamellar phase (i.e., the layer thickness, see Sec. I B) at the first-order transition point to the random bicontinuous phase also satisfies Eqs. (2.33) and (2.34). We anticipate here the physical picture of this phase transition (see Fig. 5). Upon decreasing the volume fraction of the surfactant (2.1), the layer thickness ξ, as well as the distance between collisions L_1, increases until some critical volume fraction when the validity of Eqs. (2.33) and (2.34) is reached. At this point, the bending energy cost of creating a passage (see Fig. 5) is of order T. On the other hand, the entropy increase on going from perfectly ordered lamellar [Fig. 5(a)] to random microemulsion is of order 1 per cell, i.e., the corresponding free-energy decrease is of order T per cell. Note that a passage is the same size as a unit cell as shown in Fig. 5(b). Thus, at some critical volume fraction of the surfactant, the lamellar phase melts into the random bicontinuous phase.

Let us stress the qualitative character of the present theory based on the use of relations such as Eq. (2.22), which is strictly valid for $L_1 \ll \xi_p$. We presume that this equation, describing softening of the membrane rigidity $K_M(L_1)$ remains qualitatively correct up to $L_1 \lesssim \xi_p$ [when it predicts $K(L_1)\approx T$]. This is likely to be so, since at length scales larger than ξ_p, a free fluid membrane is expected to behave as a completely crumpled object, characterized by the absence of long-range orientational order of normals erected perpendicular to local surface elements.[13] Thus, the effects of rigidity should disappear at $L_1 > \xi_p$, as is consistent with $K(\xi_p)\approx T$. In the following we presume that a reasonably good fit to the exact $K_M(L_1)$ has the form of (2.22) even for large L_1, of order but less than ξ_p. In principle, the parameter α entering this fit can be different from the previously mentioned value $\alpha=3$. The value of α for $L_1 \ll \xi_p$ might not be appropriate for $L_1 \lesssim \xi_p$.

From Eqs. (2.18) and (2.22), one can see that to a good approximation,

$$K_M(L_1)=K_{\text{eff}}(\xi)=\frac{\alpha T}{4\pi}\ln\frac{\xi_p}{\xi} \tag{2.35}$$

for $w \ll \xi \ll \xi_p$. In fact, Eq. (2.35) is the one used by Safran *et al.* in Ref. 1. Equation (2.35) is different from (2.22) since in (2.22) the argument is L_1 rather than ξ as in (2.35). Nevertheless, both formulas agree quantitatively for $w \ll \xi \ll \xi_p$, and, more importantly, qualitatively when $\xi \lesssim \xi_p$ when both formulas predict that the effective bending constant $K_M(\xi)\approx K_M(L_1)$ is of order T [Recall that for this case $\xi\approx L_1\approx\xi_p$ as indicated by Eqs. (2.33) and (2.34)].

Thus, in the following we will use Eq. (2.35) in the coarse-grained Hamiltonian (2.29). The next and the most drastic simplification we make is to set (as in previous studies[1–3]) the effective Gaussian curvature bending constant to zero:

$$K_G(L_1)=0 . \tag{2.36}$$

The assumption (2.36) is consistent with a crude approximation (Sec. II C) in which mean surfaces S_j are composed of pieces with zero Gaussian curvature so that the Gaussian curvature term (2.32) might be thought to be zero. Though, in principle, one might hope that some of the essential features of the phase diagrams can be understood within the framework of a single-bending-constant approximation, Gaussian curvature may have some interesting effects as discussed in Sec. V.[25]

Finally, we will simplify our formulas for $a(L_1)$, Eqs. (2.24) to (2.28). For $L_1 \ll \xi_p$, the second term in large parentheses of (2.25) is either small or, when $L_1 \lesssim \xi_p$, of order unity. Thus, as a qualitatively good approximation, one may take

$$\sigma_R \approx \sigma-\sigma_0=\sigma_s . \tag{2.37}$$

With the aid of (2.37), one may rewrite the steric free energy, Eq. (2.28), as

$$F_{st}=\frac{\pi T}{32\mu\alpha(\xi-w)^2\ln\frac{\xi_p}{\xi}} . \tag{2.38}$$

So, from (2.37) and (2.38) [with $w=a$ as discussed in the paragraph after Eq. (2.22′)] we have that $a(L_1)$ [Eq. (2.24)] is approximately

$$a(L_1)\approx a_{\text{eff}}(\xi)=\sigma_s+\frac{\pi T}{32\mu\alpha(\xi-a)^2\ln\frac{\xi_p}{\xi}} . \tag{2.39}$$

In conclusion, as the entries of the effective Hamiltonian (2.29), we use expressions given by Eq. (2.35), (2.36), and (2.39).

Note that $a_{\text{eff}}(\xi)$ and, consequently, the effective Hamiltonian (2.29) diverge strongly as $\xi \to a = w$. Thus the

numerator in the second term of $a_{\text{eff}}(\xi)$ provides a short-scale cutoff to ξ at $\xi_{\min}=a=w$. Most of the transitions discussed in detail in Sec. IV are not affected by this short-scale cutoff (e.g., the lamellar-to-bicontinuous phase transition described above occurs at $\xi\approx\xi_p >> a$). However, the length scale ξ in the dilute phase at the first-order transition between the random bicontinuous and dilute phases (which occurs in a range of values of α and μ as discussed in Sec. IV) is of order $\xi_{\min}$ at low T. The same result was obtained in the phenomenological treatment of Safran *et al.*[1] Though one might argue about the validity of the theory when $\xi \gtrsim a$, the fact that the length scale in the dilute phase at coexistence with the random bicontinuous phase (i.e., in the middle phase microemulsion) is of the order of some molecular length (say, the size of micelles) seems to be in agreement with experimental observations. We note that the theory of Ref. 1, rather than using the smooth cutoff procedure embedded in Eq. (2.39), imposes a hard cutoff by limiting ξ to be greater than a. Nevertheless, the properties of the dilute phases coexisting with the middle phase predicted by both our theory and that of Ref. 1 are identical. In particular, both theories predict $\xi \gtrsim a$ in the dilute phases. We will discuss this in more detail in Sec. IV where we also study the existence of the middle phase microemulsion state, which is strongly dependent on the actual values of α and μ chosen. However, it should be stressed that both the hard cutoff prescription of Ref. 1 and our smooth prescription are purely of a mathematical character.

C. Construction of the lattice model

In this subsection we proceed to construct the effective lattice Hamiltonian (2.29). The problem at hand is to estimate somehow the area $A(\{\phi_i\})$ and bending terms $B_M(\{\phi_i\})$ and $B_G(\{\phi_i\})$ [Eqs. (2.30)–(2.32)] which are sums of integrals over smooth mean interfaces $\{S_j\}$ between water ($\phi_i=0$) and oil ($\phi_i=1$) domains.

One possible strategy is to start from ordinary Ising interfaces [Fig. 8(a)] on a cubic lattice contributing ξ^2 to $A(\{\phi_i\})$ [Eq. (2.30)] for each bond $\langle ij \rangle$ connecting nearest-neighbor sites occupied by different liquids. Then, it is easy to see that

$$A(\{\phi_i\})=\xi^2 \sum_{\langle i,j \rangle} N_{\langle ij \rangle} , \tag{2.40}$$

where $N_{\langle ij \rangle}$ is the occupation number of broken bonds,

$$N_{\langle ij \rangle}=\phi_i(1-\phi_j)+(1-\phi_i)\phi_j , \tag{2.41}$$

which is 1 if the the $\langle ij \rangle$ bond is broken and zero if it is not.

A problem arises when one wants to estimate bending terms, Eqs. (2.31) and (2.32). A natural step is somehow to smooth the sharp edges of Ising interfaces (which are plaquettes of the lattice which is dual to the lattice of spins ϕ_i), as indicated in Fig. 8(b): each edge is replaced by one-quarter of a cylinder with radius $\xi/2$ and height ξ [contributing $\pi/2$ to $B_M(\{\phi_i\})$ and nothing to $B_G(\{\phi_i\})$ because the Gaussian curvature of a cylindrical surface is zero] while corners are approximated by $\frac{1}{8}$ of a sphere with radius $\xi/2$ [contributing π to $B_M(\{\phi_i\})$, and $\pi/2$ to $B_G(\{\phi_i\})$]. However, ambiguities in the smoothing process appear when one wants to smooth more complex configurations like the one in Fig. 8(c). Thus, it is difficult to propose a good and simple smoothing process for estimating $B_M(\{\phi_i\})$.[26]

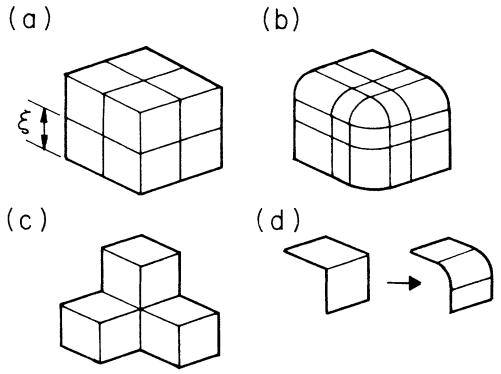

FIG. 8. To estimate the bending energy of mean interfaces, sharp edges and corners of Ising interfaces in (a) are smoothed in (b). There is no simple way to smooth Ising interfaces in (c). (d) We use smoothing which removes only sharp edges of Ising interfaces.

In the following we confine ourselves to an extremely simple smoothing process which consists of associating with each sharp edge of the unsmoothed interface a contribution of $\pi/2$ to $B_M(\{\phi_i\})$. This corresponds to the aforementioned replacement of an edge by one-quarter of a cylinder [giving zero contribution to $B_G(\{\phi_i\})$] as shown in Fig. 8(d). We decided not to include any contribution to a $B_M(\{\phi_i\})$ from more complex situations such as the corner in Fig. 8(a). Thus, our scheme is, basically, to associate the contribution $\Delta B=\pi/2$ to each pair of plaquettes of the unsmoothed interface which share a common sharp edge [Fig. 8(d)]. Accordingly, a single oil cube immersed in water background gives

$$B_M(\{\phi_i\})=12\Delta B=6\pi , \tag{2.42}$$

while in the framework of the smoothing approach described in the preceding paragraph (which is unambiguous for this simple case), the cube is smoothed into a sphere of radius $\xi/2$ giving

$$B_M(\{\phi_i\})=8\pi . \tag{2.43}$$

Though the difference between 6π, Eq. (2.42), and 8π, Eq. (2.43), might seem not so important (corresponding to other quantitative uncertainities, as those of Sec. II B), we shall try in the following to elucidate possible effects of such an uncertainty by introducing a new phenomenological parameter m such that the contribution of a sharp edge to $B_M(\{\phi_i\})$ is

$$\Delta B=\frac{m\pi}{3} . \tag{2.44}$$

When

$$m=\tfrac{3}{2} , \tag{2.45}$$

this reduces to the previous choice with $\Delta B=\pi/2$. When

$$m=2\ , \tag{2.46}$$

the contribution of a single cube is

$$B_M(\{\phi_i\})=12\Delta B=8\pi\ , \tag{2.47}$$

coinciding with Eq. (2.43), which is obtained by a more sophisticated smoothing turning the cube into a sphere.

There are some more fundamental reasons for the introduction of the parameter m. First, note that by Eqs. (2.35) and (2.44), the bending-energy contribution $K_{\rm eff}(\xi)B_M(\{\phi_i\})$ of a single oil cube in water is

$$12\Delta BK_{\rm eff}(\xi)=m\alpha T\ ln(\xi_p/\xi)\ . \tag{2.48}$$

Thus, some uncertainty of α may be absorbed into an uncertainty in m (recall that, as discussed in Sec. II B, the value of α appropriate for $\xi\ll\xi_p$ might not be appropriate when $\xi\lesssim\xi_p$). Actually, as demonstrated in the following, α will enter the final form of the effective Hamiltonian either in the combination $m\alpha$ or in the combination $(\mu\alpha)^{-1}$. In Sec. IV we will present phase diagrams for various values of these two phenomenological parameters.

The second reason for introducing m is illustrated in Fig. 9, which shows that for a cluster consisting of a large number of blocks, the smoothing process (though, for this particular situation, unambiguous) overestimates bending energy: the spurious anisotropy introduced by the use of the cubic lattice requires that the tilted interface in Fig. 9 be approximated by a "staircase." On the other hand, in microemulsions, there are no preferred directions, and it would be more natural to approximate the tilted interface by a planar one (as done with the horizontal and vertical interfaces in Fig. 9). Thus, in general, even a more sophisticated smoothing approach would overestimate the actual bending-energy because of lattice anisotropy. However, as shown in the following, the bending energy contribution to $H(\{\phi_i\})$ is proportional to $m\alpha$. Thus, this contribution can be somewhat lessened by choosing smaller values of m than those in Eqs. (2.45) and (2.46).

Now, we proceed to write down the final expression for $B_M(\{\phi_i\})$ in terms of $\{\phi_i\}$ by associating the contribution ΔB of Eq. (2.44) to each sharp edge of the unsmoothed lattice. This is unambiguous if the edge is shared by just two plaquettes of the unsmoothed interface [Fig. 10(a)]. However, if four plaquettes share the same edge, there are two ways to smooth [see Fig. 10(b)]. Since we presume zero spontaneous curvature r_0^{-1}, contributions of both configurations to $B_G(\{\phi_i\})$ are equal. Thus, for $r_0^{-1}=0$, one has to count bends, as indicated in Figs. 10(c)–10(f). Let us denote by $N_{\langle ijkl\rangle}$ the number of bends associated with various configurations of four spins ϕ_i, ϕ_j, ϕ_k, and ϕ_l surrounding a bond of the lattice which is dual to the lattice of spins [see Fig. 10(c)]. This spin operator can be only 0 [Fig. 10(d)], 1 [Figure 10(e)], or 2 [Fig. 10(f)]. It is easy to check that the unique spin operator counting the number of bends is

$$\begin{aligned}N_{\langle ijkl\rangle}=&N_{\langle il\rangle}N_{\langle ji\rangle}+N_{\langle ji\rangle}N_{\langle kj\rangle}+N_{\langle kj\rangle}N_{\langle lk\rangle}\\&+N_{\langle lk\rangle}N_{\langle il\rangle}-2N_{\langle il\rangle}N_{\langle ji\rangle}N_{\langle kj\rangle}N_{\langle lk\rangle}\ ,\end{aligned} \tag{2.49}$$

where $N_{\langle il\rangle}$ is given by (2.41). Note that both $N_{\langle ij\rangle}$ and $N_{\langle ijkl\rangle}$ are invariant with respect to the global symmetry $\phi_i\rightarrow 1-\phi_i$. Each bend contributes ΔB [Eq. (2.44)] to $B_M(\{\phi_i\})$. So

$$B_M(\{\phi_i\})=\tfrac{1}{3}m\pi\sum_{\langle i,j,k,l\rangle}N_{\langle ijkl\rangle}\ , \tag{2.50}$$

where the sum runs over the bonds of the lattice which is dual to the lattice of spins or, equivalently, over the plaquettes of the original lattice [Fig. 10(c)].

A generalization of the theory to the case of nonzero spontaneous curvature would not be trivial—it would require additional two-state (i.e., Ising) variables to distinguish between two sets of smooth interfaces $\{S_j\}$ in Fig. 10(b) (or in Fig. 3) corresponding to a given spin configuration $\{\phi_i\}$. These variables have to live on the bonds of the dual lattice. When $r_0^{-1}=0$, the effect of these variables is trivial because the two configurations in Fig. 3 give equal contributions to $B_M(\{\phi_i\})$ for $r_0^{-1}=0$. For general $r_0^{-1}\neq 0$, one can show that these new variables can be integrated out of the partition function. The resulting Hamiltonian is not invariant with respect to global Ising symmetry $\phi_i\rightarrow 1-\phi_i$. Thus, nonzero r_0^{-1}

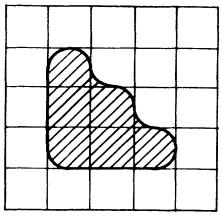

FIG. 9. Spurious spatial anisotropy of the cubic lattice causes an overestimate of the bending energy.

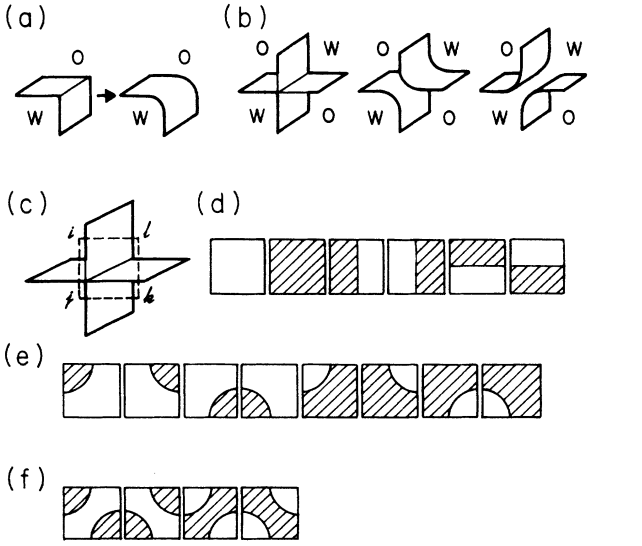

FIG. 10. (a) When an edge is shared by two plaquettes there is a unique way of smoothing. (b) When four plaquettes share a single edge, there are two ways of smoothing. (c) Four spins surrounding a bond of a dual lattice. (d)–(f) give configurations of mean interfaces corresponding to various configurations of four spins in (c). Oil regions are hatched.

breaks the symmetry between oil and water. Of course, this symmetry breaking vanishes when $r_0^{-1} \to 0$. The presence of arbitrarily small spontaneous curvature is, however, of importance in interpreting the phases of the lattice model for microemulsions. Thus, e.g., by smoothing the columnar phase of the spin model [Fig. 4(b)], one may obtain two tubular phases in the system with $V_o = V_w$: either tubes of oil in a water background or vice versa. Depending on its sign, a small nonzero value of r_0^{-1} would favor one or the other of these phases. At $r_0^{-1} = 0$ the two phases coexist and correspond to a single columnar phase of the lattice model. Similarly the antiferromagnetic phase of the spin model [Fig. 4(c)] may correspond to two fcc droplet crystals (oil droplets in water and vice versa) coexisting at $r_0^{-1} = 0$.

Let us note that a third set of additional Ising variables might be needed to resolve the smoothing "uncertainty" illustrated in Fig. 11. These new variables have to live on sites of the dual lattice. Both these and the previously mentioned additional variables assist in resolving situations where more than one set of smooth interfaces $\{S_j\}$ can be associated with a given spin configuration $\{\phi_i\}$. Actually a more complete theory including Gaussian curvature effects has to account for these variables living on sites and bonds of the dual lattice (e.g., note that two smoothed configurations which can be associated with unsmoothed cubes in Fig. 11 have different topology and thus different Gaussian curvature energies).

In the following we will confine ourselves to balanced microemulsions, i.e., to systems of fluid membranes which have zero spontaneous curvature, $r_0^{-1} = 0$, and to the simple prescription for counting bends imbedded in Eq. (2.50). In the single bending constant approximation [which presumes $K_G(L_1) = 0$, Eq. (2.36), or, equivalently, $B_G(\{\phi_i\}) = 0$, as explained above], the coarse-grained lattice Hamiltonian (2.29), can be written by means of Eqs. (2.40) and (2.50) as

$$H(\{\phi_i\}) = \xi^2 a(L_1) \sum_{\langle i,j \rangle} N_{\langle ij \rangle} + \frac{\pi m}{3} K_M(L_1) \sum_{\langle i,j,k,l \rangle} N_{\langle ijkl \rangle} . \tag{2.51}$$

Spin operators $N_{\langle ij \rangle}$ and $N_{\langle ijkl \rangle}$ entering (2.51) are defined respectively by Eqs. (2.41) and (2.49). The first sum in (2.51) runs over bonds of the lattice of spins ϕ_i, while the second one runs over plaquettes, as discussed above. Parameters $a(L_1)$ and $K_M(L_1)$ in (2.51) are, eventually, functions of the cell size ξ [see Eqs. (2.18), (2.22), and (2.24)–(2.27)]. As the next step, one has to insert the Hamiltonian (2.51) into the partition function (2.13) in order to obtain the free-energy density $F(\sigma, \mu_o, \xi)$, which after minimization over ξ gives the phenomenological free-energy density $F(\sigma, \mu_o)$, as indicated in Eq. (2.15). Let us elucidate the meaning of this minimization in the example of a state, depicted in Fig. 5(a), which is very close to a perfectly ordered lamellar microemulsion. For such a state all $N_{\langle ijkl \rangle} \approx 0$, while $N_{\langle ij \rangle}$ is approximately 1 if ϕ_i and ϕ_j belong to neighboring layers and zero otherwise, and

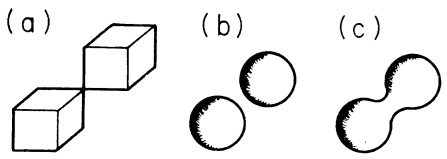

FIG. 11. The two unsmoothed cubes in (a) may correspond to smooth configurations in (b) and (c).

$$\frac{1}{V} \sum_{\langle i,j \rangle} N_{\langle ij \rangle} = \frac{1}{\xi^3} , \qquad \frac{1}{V} \sum_{\langle i,j,k,l \rangle} N_{\langle ijkl \rangle} = 0 .$$

Then $F(\sigma, \mu_o = 0, \xi)$ is approximately $H(\{\phi_i\})/V$, and

$$F(\sigma, \mu_o = 0, \xi) = a(L_1)/\xi, \tag{2.52a}$$

or

$$F(\sigma, \mu_o = 0) = [a(L_1)/\xi]_{\min(\xi)} \tag{2.52b}$$

for perfectly ordered lamellar microemulsion with $V_o = V_w$, i.e., $\mu_o = 0$. Equations (2.52) were derived recently in Ref. 15 in a theory of smectic elastic constants of lamellar multimembrane systems. As explained there, the thermal equilibrium smectic state of these phases (the one satisfying the Landau-Peierls theorem) is achieved when the function (2.52a) is minimal with respect to variation in ξ, the layer thickness. Here, we presume by Eq. (2.15) that this variational principle is valid in general, not only in the special case of perfectly ordered lamellar phase. Thus, the lattice size ξ, which was initially an artifact of the phenomenological approach, is naturally chosen by demanding that the system be an equilibrium state.

In the following we will use the Hamiltonian (2.51) with entries $a(L_1)$ and $K_M(L_1)$ approximated, respectively, by Eqs. (2.39) and (2.35):

$$H(\{\phi_i\}) = \xi^2 \left[\sigma_s + \frac{\pi T}{32 \mu \alpha (\xi - a)^2 \ln(\xi_p/\xi)} \right] \sum_{\langle i,j \rangle} N_{\langle ij \rangle} + \tfrac{1}{12} m \alpha T \ln(\xi_p/\xi) \sum_{\langle i,j,k,l \rangle} N_{\langle ijkl \rangle} . \tag{2.53}$$

As previously anticipated, there are two phenomenological parameters, $\mu\alpha$ and $m\alpha$, entering (2.53). The sensitivity of the phase diagram to the variation of these parameters is discussed in Sec. IV.

III. MEAN-FIELD THEORY

A. Variety of microemulsion phases within mean-field theory

In this section we construct a mean-field theory in order to calculate approximately the free-energy density $F(\sigma, \mu_o = 0)$ given by Eqs. (2.13) and (2.15) as

$$F(\sigma, \mu_o = 0) = \left[-\frac{T}{V} \ln \mathrm{Tr}_{\{\phi_i\}} \exp \left[\frac{-H(\{\phi_i\})}{T} \right] \right]_{\min(\xi)} , \tag{3.1}$$

with $H(\{\phi_i\})$ as in Eq. (2.53). In (3.1) we restricted ourselves to the states characterized by $\mu_o=0$. The magnetic field term

$$-\mu_o\xi^3\sum_i\phi_i$$

in Eq. (2.13) is the only one which breaks the global symmetry $\{\phi_i\}\rightarrow\{1-\phi_i\}$ of $H(\{\phi_i\})$. As observed in Sec. II C, $H(\{\phi_i\})$ has this symmetry because we restricted ourselves to balanced microemulsions (zero spontaneous curvature r_0^{-1}) which are symmetric with respect to exchanging water and oil domains. Our quantitative results with $\mu_o=0$, presented in Sec. IV in terms appropriate for microemulsions, are also applicable to binary systems composed of surfactant bilayers in a single solvent, water or oil.[2] These systems are naturally characterized by zero spontaneous curvature and are essentially indistinguishable from balanced microemulsions.[2] For concreteness in the following, we will use language appropriate for microemulsion systems. In this language the states we are interested in, characterized by $\mu_o=0$ are (a) those which are invariant under exchange of oil and water cells [i.e., the paramagnetic phase, depicted in Fig. 1(b), corresponding to the random bicontinuous microemulsion with $V_o=V_w$], (b) states which are invariant with respect to this exchange accompanied by a discrete translation (i.e., the periodic lamellar, columnar, and antiferromagnetic phases of the spin system describing a microemulsion system with $V_o=V_w$). In addition to these states, we will study the ferromagnetic phases of the model which correspond to diluted oil- and water-rich phases in which the oil-water symmetry is spontaneously broken. These two phases coexist when $\mu_o=0$ just as the up and down phases of an Ising ferromagnet coexist in a zero magnetic field [Fig. 1(a)].

We anticipate that the phase behavior found in this paper is basically that of an Ising model with competing interactions. Our work can be seen as a bridge between the phenomenological approach of Refs. 1–3 and the lattice theories of microemulsions of Schick and co-workers and others[27] which predict diagrams similar to ours. In our study, we focus mostly on the zero magnetic field case $m_0=0$, thus obtaining phase behavior of balanced microemulsions corresponding to the 1:1 oil-to-water volume ratio cross section of the ternary oil-water-surfactant phase diagram[1–3] (see Sec. IV). In this case, it is appropriate to label the paramagnetic phase as the bicontinuous (B) phase. In the presence of nonzero uniform field, this phase continuously evolves to a mostly oil phase (at large positive μ_o) or to a mostly water phase (at large negative μ_o).

In the following we calculate the free energy (3.1) in mean field theory, which, as usual, presumes that the spin probability distribution function can be approximated by

$$P_0(\{\phi_i\})=\prod_i P_i(\phi_i)\ , \tag{3.2}$$

with $P_i(1)=\psi_i=1-P_i(0)$, so that $\langle\phi_i\rangle_0=\psi_i$ with $0\le\psi_i\le1$. Then, the mean-field approximation to Eq. (3.1) reads [28]

$$F(\sigma,\mu_o=0)=\frac{1}{V}[\langle H(\{\phi_i\})\rangle_0-TS_0]_{\min(\xi,\{\psi_i\})}\ , \tag{3.3}$$

where $\langle\ \rangle_0$ denotes the average with respect to the distribution (3.2), and S_0 is the entropy:

$$S_0=-\sum_i[\psi_i\ln\psi_i+(1-\psi_i)\ln(1-\psi_i)]\ . \tag{3.4}$$

Note that the mean-field approximation to the free-energy density is obtained by minimizing Eq. (3.3) with respect to both $\{\psi_i\}$ and ξ at constant V and σ.

As anticipated in the Introduction, the uniform diluted (D) and bicontinuous (B) phases are characterized by i-independent $\langle\phi_i\rangle=\psi_i$:

$$\psi_i=\phi, \tag{3.5a}$$

with

$$\phi=\tfrac{1}{2} \tag{3.5b}$$

for the paramagnetic, i.e., the B phase, and $\phi>\frac{1}{2}(\phi<\frac{1}{2})$ for the ferromagnetic, i.e., the oil (water) rich D phase. Thus, the ferromagnetic ordering is characterized by a spatially uniform, i.e., i-independent order parameter $\psi_i-\frac{1}{2}=\phi-\frac{1}{2}$. Periodic phases have an i-dependent order parameter $\psi_i-\frac{1}{2}$, e.g., the lamellar phase (L) has

$$\psi_i=\phi \tag{3.6a}$$

when i is in even ("oil") layers, and

$$\psi_i=1-\phi \tag{3.6b}$$

when i is in odd ("water") layers of thickness ξ [Fig. 4(a)]. A perfectly ordered L phase [Fig. 5(a)] results when $\phi=1$ or $\phi=0$ in Eqs. (3.6). The columnar phase (C) is defined in a similar way, with Eq. (3.6a) satisfied in "oil" columns and Eq. (3.6b) satisfied in "water" columns of side ξ [see Fig. 4(b)]. In the antiferromagnetic phase (A) [Fig. 4(c)], the cubic lattice is divided into two interpenetrating sublattices of "oil" and "water" cells of side ξ with Eq. (3.6a) satisfied in the "oil" cells and Eq. (3.6b) in the "water" cells. Thus nearest-neighbor cells of the original lattice are different and next-nearest neighbors the same. These periodic phases are perfectly ordered when $\phi=1$ (or 0) in Eqs. (3.6). In equilibrium at nonzero temperature, thermally excited defects will reduce ϕ from its saturation value of 1 (or increase it from 0). Long-range translational order persists, however, until $\phi=\frac{1}{2}$ when the uniform bicontinuous phase is regained as indicated by the equivalence of Eq. (3.6) and (3.5) in this limit.

By Eqs. (3.5) and (3.6) it is easy to see that for all phases we consider (B, D, L, C, and A phase),

$$S_0=-\frac{V}{\xi^3}[\phi\ln\phi+(1-\phi)\ln(1-\phi)]\ , \tag{3.7}$$

which is a standard expression for the entropy of mixing. The difference in free energy among the various phases comes from $\langle H(\{\phi_i\})\rangle_0$ in Eq. (3.3), which by Eq. (2.53) is conveniently expressed as

$$\frac{\langle H(\{\phi_i\})\rangle_0}{V}=\frac{1}{\xi}\left[\sigma_s+\frac{\pi T}{32\mu\alpha(\xi-a)^2\ln(\xi_p/\xi)}\right]A_N(\phi)+\frac{1}{\xi^3}\frac{m\alpha T}{12}\ln(\xi_p/\xi)B_N(\phi)\ , \tag{3.8}$$

with $N=B$, D, L, C, and A, while $A_N(\phi)$ and $B_N(\phi)$ are defined by

$$A_N(\phi)=\frac{\xi^3}{V}\left\langle \sum_{\langle i,j\rangle} N_{\langle ij\rangle}\right\rangle_{0,N} \tag{3.9}$$

and

$$B_N(\phi)=\frac{\xi^3}{V}\left\langle \sum_{\langle i,j,k,l\rangle} N_{\langle ijkl\rangle}\right\rangle_{0,N} \tag{3.10}$$

with averages performed with respect to the N phase [defined by Eqs. (3.5) and (3.6), respectively, for uniform and periodic phases]. It is easy to see that $A_N(\phi)$ and $B_N(\phi)$ are ξ independent. It is less trivial but, nevertheless, straightforward to calculate them. Here we give the results for various phases N. They are all of the form

$$A_N(\phi)=A_N^{(0)}+A_N^{(1)}\phi(1-\phi), \tag{3.11}$$

and

$$B_N(\phi)=B_N^{(0)}+B_N^{(1)}\phi(1-\phi)+B_N^{(2)}[\phi(1-\phi)]^2\ , \tag{3.12}$$

with constants $A_N^{(i)}$ and $B_N^{(i)}$ given in Table I. $A_N(\phi)$ and $B_N(\phi)$ in Eqs. (3.11) and (3.12) are given in Fig. 12. From this figure one can see that $A_N(\phi=\frac{1}{2})$, as well as $B_N(\phi=\frac{1}{2})$ are equal for various phases N as they should be: the state with $\phi=\frac{1}{2}$ is the limit in which all the phases become identical to random bicontinuous phase, Eq. (3.5b).

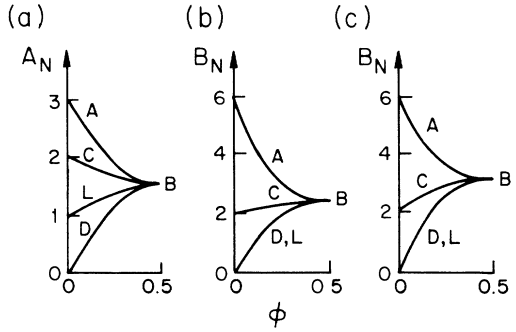

FIG. 12. The area (a) and bending (b) structure factors. (c) gives the approximate bending structure factor we use in our calculations. Because of the symmetry under $\phi\to 1-\phi$, curves are given only for $0<\phi<\frac{1}{2}$. The limit $\phi=\frac{1}{2}$ correspond to random bicontinuous phase (B). D indicates the dilute, L the lamellar, C the columnar, and A the antiferromagnetic phase.

Thus, to summarize, by Eqs. (3.7) to (3.12), the mean-field free-energy density (3.3) can be written as

$$F(\sigma,\mu_o=0)=[\Phi(N,\xi,\phi)]_{\min(N,\xi,\phi)}\ , \tag{3.13a}$$

with

$$\Phi(N,\xi,\phi)=\frac{1}{\xi}\left[\sigma_s+\frac{\pi T}{32\mu\alpha(\xi-a)^2\ln(\xi_p/\xi)}\right][A_N^{(0)}+A_N^{(1)}\phi(1-\phi)]+\frac{1}{\xi^3}\frac{m\alpha T}{12}[\ln(\xi_p/\xi)]\{B_N^{(0)}+B_N^{(1)}\phi(1-\phi)+B_N^{(2)}[\phi(1-\phi)]^2\}+\frac{1}{\xi^3}T[\phi\ln\phi+(1-\phi)\ln(1-\phi)] \tag{3.13b}$$

and $A_N^{(i)}$ and $B_N^{(i)}$ as in Table I. So, the problem is to minimize the function $\Phi(N,\xi,\phi)$ with respect to continuous variables $\xi(a<\xi<\xi_p)$ and $\phi(0<\phi<1)$ and then to determine the dominant phase by identifying the N for which $[\Phi(N,\xi,\phi)]_{\min(\xi,\phi)}$ is minimal. In this way one obtains the phase diagrams which (for fixed values of the phenomenological parameters $\mu\alpha$ and $m\alpha$) can be represented in terms of just two thermodynamic parameters, e.g., the reduced surface tension σ_s/T and inverse reduced rigidity $T/K_M(a)$, as discussed in more detail in the following.

An interesting property is the volume fraction of the surfactant [Eq. (2.1)]. For typical microemulsion systems of interest, it is only a few percent. Equations (2.1), (2.10), and (3.13) imply that the equilibrium surfactant volume fraction in mean-field theory is

$$\phi_s=\frac{a}{\xi}A_N(\phi)=\frac{a}{\xi}[A_N^{(0)}+A_N^{(1)}\phi(1-\phi)]\ , \tag{3.14}$$

where ϕ and ξ are determined by $\partial\Phi/\partial\xi=0$ and $\partial\Phi/\partial\phi=0$. Equation (3.14) will be of importance in Sec. IV for construction of phase diagrams in the $(T/K_M(a),\phi_s)$ plane (see Fig. 13).

Details of phase diagrams will be presented in Sec. IV. However, even without detailed calculations, some of the features of these diagrams can be conjectured from Eq. (3.13) and Fig. 12. In the region of the negative surface tension σ_s, the periodic phase having maximal $A_N(\phi=0)$ is strongly favored by the first or area term in (3.13b). This is, in fact, the antiferromagnetic phase [see Fig. 12(a)]. The columnar phase is also favored by the area term but less than the antiferromagnetic phase. The di-

TABLE I. Constants entering area and bending structure factors.

N	$A_N^{(0)}$	$A_N^{(1)}$	$B^{N(0)}$	$B_N^{(1)}$	$B_N^{(2)}$
D	0	6	0	12	-12
L	1	2	0	12	-12
C	2	-2	2	4	-12
A	3	-6	6	-12	-12

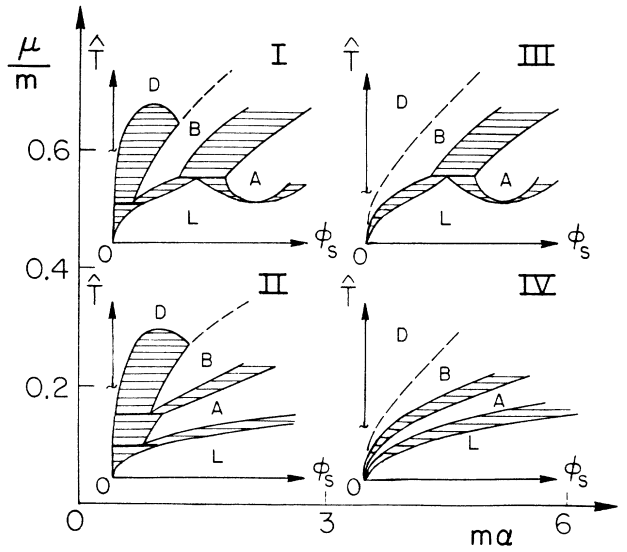

FIG. 13. Four types of ($\phi_s, \hat{T}$) phase diagrams obtained from our model. Diagrams are schematic. The typical scale for ϕ_s is of $O(10\%)$ while that for $\hat{T}$ is $O(1)$. The phases shown are the ferromagnetic or dilute (D), the paramagnetic or bicontinuous (B), the lamellar (L), and antiferromagnetic (A) phases. Tie lines in the coexistence regions are indicated by horizontal hatching. The DB critical line is dashed.

lute and lamellar phases are disfavored by the area term alone. Thus in the absence of the second or bending term in (3.13b) the antiferromagnetic phase would dominate the negative surface tension region. On the other hand, the bending term in (3.13) strongly disfavors the antiferromagnetic phase, while favoring the dilute, lamellar, and, to a lesser extent, the columnar phase [see Table I and Fig. 12(b); note that, accidentally, the bending functions of the dilute and lamellar phases coincide: $B_L(\phi)=B_D(\phi)$]. Thus, the bending term of (3.13) [proportional to $K_{\rm eff}(\xi)$, Eq. (2.35)] can be expected to be of importance in determining which of the periodic phase wins in the negative surface tension region. Thus, one may expect that the heavily curved antiferromagnetic phase (interpreted as a droplet crystal in Sec. II C) will dominate in the high-T portion of the negative surface tension region [where $K_{\rm eff}(\xi)/T$ is relatively small]. On the other hand, in the low-T portion [high $K_{\rm eff}(\xi)/T$] one expects the dominance of the lamellar phase, which obviously costs no bending energy [cf., Fig. 12(b), $B_L(0)=B_L(1)=0$]. These conjectures are confirmed quantitatively in Sec. IV. The situation in the region of the low surface tension σ_s in Eq. (3.13) is more subtle and is discussed in Sec. IV. Finally, positive σ_s strongly favors the dilute phase via the area term in (3.13) [see Fig. 12(a)]. Thus, at least in the low-T region, one may expect phase separation, i.e., the dominance of the dilute phase.

B. Possible extensions of the phenomenological theory and an additional approximation

The constants $A_N^{(i)}$ and $B_N^{(i)}$ in Eq. (3.3b) can also be treated in a phenomenological manner—as adjustable parameters to be determined to reach agreement with experimental observations (or with results of more rigorous theoretical approaches). Thus one may exploit the expansion

$$B_N(\phi)=\sum_{n=0}^{\infty} B_N^{(n)}[\phi(1-\phi)]^n \tag{3.15}$$

[and a similar one for $A_N(\phi)$] with constants $B_N^{(i)}$ to be considered as phenomenological parameters. Similarly, one may introduce the effects of Gaussian curvature, which are completely neglected in this paper. The constants $B_N^{(i)}$ are not completely arbitrary. Thus, e.g., $B_N(\phi)$ [as well as $A_N(\phi)$] have to be equal for all N when $\phi=\frac{1}{2}$ since all phases reduce to the B phase in this case. Also, there is no bending energy in perfectly ordered L and D phases so that $B_N(\phi=1)=0$ (i.e., $B_N^{(0)}=0$) when $N=L$ or D. In completely diluted phases, there are no surfaces implying $A_D^{(0)}=0$. Also, it is easy to see that $A_L^{(0)}=A_L(\phi=1)$ has to be 1.

With these remarks in mind, we decided to simplify our calculations by setting

$$B_N^{(2)}=0\ , \tag{3.16}$$

which is equivalent to dropping the $[\phi(1-\phi)]^2$ term in Eq. (3.13b). Also, we decided to retain the parameters $B_N^{(i)}$ and $A_N^{(i)}$, $i=0$, 1, as given in Table I. This simplification does not violate any of the general principles discussed in the preceding paragraph. Moreover, none of the trends in phase diagrams we described in Sec. III A is altered [see Fig. 12(c) for comparison with the previous curves with $B_N^{(2)}\neq 0$, which are given in Fig. 12(b)], since the bending energy still favors D, L, and C phases while disfavoring the A phase.

In choosing (3.16) we have not been led by any of the phenomenological data. The basic reasons for (3.16) are the following: first, when $B_N^{(2)}=0$, the ϕ dependence of (3.13b) is identical to that of the mean-field free energy of a nearest-neighbor Ising model. This simplifies minimization over ϕ at fixed ξ, as well as visualization of the results. Thus, by defining a ξ -dependent "exchange" constant,

$$J_N(\xi)=\frac{1}{2}\left[\frac{\sigma_s\xi^2}{T}+\frac{\pi}{32\mu\alpha(1-a/\xi)^2\ln(\xi_p/\xi)}\right]A_N^{(1)} + \frac{m\alpha}{24}[\ln(\xi_p/\xi)]B_N^{(1)}, \tag{3.17}$$

it is easy to see that for

$$J_N(\xi) < 1\ , \tag{3.18}$$

the minimum of $\Phi(N,\xi,\phi)$ with respect to ϕ occurs at $\phi=\frac{1}{2}$. Thus, when ξ is in a range in which (3.18) is satisfied, the length-scale-dependent free-energy density of the N phase,

$$\Phi(N,\xi)\equiv[\Phi(N,\xi,\phi)]_{\min(\phi)}\ , \tag{3.19}$$

coincides with that of the B phase:

$$\Phi(B,\xi)=\Phi(N,\xi,\phi=\tfrac{1}{2})\ . \tag{3.20}$$

On the other hand, when

$$J_N(\xi) > 1 , \tag{3.21}$$

the curve $\Phi(N,\xi)$ bifurcates from $\Phi(B,\xi)$. Competition between various phases is easy to visualize in terms of functions $\Phi(N,\xi)$ (see Sec. IV). Note that by (3.19) and (3.13a),

$$F(\sigma,\mu_o=0)=[\Phi(N,\xi)]_{\min(N,\xi)} . \tag{3.22}$$

Thus the dominant phase N is determined by the function $\Phi(N,\xi)$ which has the deepest minimum as a function of ξ.

The second motivation for (3.16) is more of an historical one. With this choice of $B_N^{(2)}$, our mean-field theory [Eq. (3.13b)] when applied to uniform phases reduces to that of Ref. 1 when $m=2$, $\alpha=1$, and steric entropy is switched off $1/\mu=0$. Some comparison with Ref. 1 will be made later.

C. Dimensionless form of the mean-field theory

Finally, it is useful to introduce dimensionless parameters

$$y=\xi/\xi_p , \tag{3.23}$$

$$\mu_s=-\sigma_s\xi_p^2/T , \tag{3.24}$$

and

$$z=a/\xi_p=\exp[-4\pi K_M(a)/\alpha T] . \tag{3.25}$$

Then by Eqs. (3.13) and presuming (3.16),

$$F(\sigma,\mu_o=0)=\frac{T}{\xi_p^3}[\tilde{\Phi}(N,y,\phi)]_{\min(N,y,\phi)} \tag{3.26}$$

with

$$\tilde{\Phi}(N,y,\phi)=\frac{1}{y^3}\left\{\left[-\mu_s y^2+\frac{\pi}{32\mu\alpha(1-z/y)^2\ln(1/y)}\right][A_N^{(0)}+A_N^{(1)}\phi(1-\phi)] + \frac{\mu\alpha}{12}[\ln(1/y)][B_N^{(0)}+B_N^{(1)}\phi(1-\phi)]+\phi\ln\phi+(1-\phi)\ln(1-\phi)\right\} . \tag{3.27}$$

Note that, by Eq. (3.24), $\sigma_s<0$ corresponds to $\mu_s>0$, and vice versa. To summarize, phase diagrams can be obtained by minimizing $\tilde{\Phi}(N,y,\phi)$ with respect to y, ϕ, and N with $z<y<1$, $0<\phi<1$, and $N=B$, D, L, C, and A, and can be expressed in terms of the two parameters μ_s and z defined in Eqs. (3.24) and (3.25). In analogy with Eq. (3.19), it is useful to define the dimensionless length-scale-dependent free-energy density via

$$\tilde{\Phi}(N,y)=[\tilde{\Phi}(N,y,\phi)]_{\min(\phi)} . \tag{3.19'}$$

The dominant phase N is one with the minimum value of $[\tilde{\Phi}(N,y)]_{\min(y)}$.

The parameter z enters (3.27) only through the expression $(1-z/y)^2=(1-a/\xi)^2$, which is close to unity when $a\ll\xi$. After replacing this expression by unity, (3.27) depends only on μ_s and not on z, and one concludes that phase boundaries between two phases which both have $a\ll\xi$ at the transition occur along a vertical line $\mu_s=$ const in the (μ_x,z) plane [the $(1-z/y)^{-2}$ term in Eq. (3.27) produces a finite slope of these boundaries as exhibited in Figs. 14–18]. For such a transition, the reduced surface tension σ_s/T is by Eq. (3.24) of order of ξ_p^{-2}; thus, it is small at low T when ξ_p is large or, equivalently, z [Eq. (3.25)] is small. However, as discussed in Sec. IV, not all of the transitions are of this type.

Finally, in terms of y and z, the surfactant volume fraction (3.14) reads

$$\phi_s=\frac{z}{y}A_N(\phi)=\frac{z}{y}[A_N^{(0)}+A_N^{(1)}\phi(1-\phi)] , \tag{3.28}$$

while the ξ-dependent exchange constant, Eq. (3.17), is expressed as

$$J_N(\xi)\equiv\tilde{J}_N(y)=\frac{1}{2}\left[-\mu_s y^2+\frac{\pi}{32\mu\alpha(1-z/y)^2\ln(1/y)}\right]A_N^{(1)}+\frac{m\alpha}{24}[\ln(1/y)]B_N^{(1)} . \tag{3.29}$$

IV. GLOBAL PHASE DIAGRAMS OF MICROEMULSIONS

A. Summary of results

In the study of phase diagrams we focused on the most interesting manifold (for balanced systems) with $\mu_o=0$.[1–4] Thus, we obtain phase diagrams of balanced microemulsions corresponding to the cross section of the ternary oil-water-surfactant phase diagram with a 1:1 oil-to-water volume ratio. As explained in Sec. III, phase diagrams can either be presented as a function of chemical potential in the (μ_s,z) plane or as a function of surfactant concentration in the (ϕ_s,z) or $(\phi_s,\hat{T})$ plane where $\hat{T}=T/K(a)=4\pi/[\alpha\ln(1/z)]$.

We first summarize our results. Their details are explained in the following section. Our coarse-grained model depends on two phenomenological parameters $m\alpha$

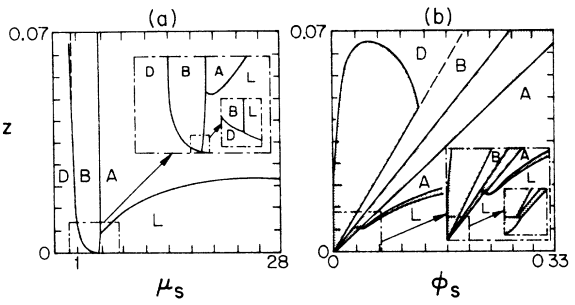

FIG. 14. (a) Type I phase diagram in the (μ_s,z) plane for $m\alpha=2.64$ and $\mu/m=0.38$. Insets give the regions in which two multiple points occur. (b) The same in the (ϕ_s,z) plane. In this figure and in Figs. 15–18, coexistence regions with horizontal tie lines are shaded.

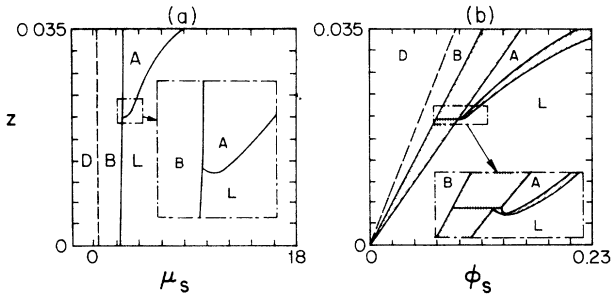

FIG. 16. (a) Type III phase diagram in the (μ_s,z) plane for $m\alpha=3.18$ and $\mu/m=043$. The inset magnifies the D-B-A triple point. (b) The same in the (ϕ_s,z) plane.

and $\mu\alpha$ [see Eq. (3.27)] whose values are to some extent uncertain, as discussed in Sec. II. Thus the form of phase diagrams depends on two dimensionless phenomenological parameters, e.g., on $m\alpha$ and μ/m, as depicted in Fig. 13, which presents the basic types of diagrams we find in the $(\phi_s, \hat{T})$ plane. This figure encompasses the range of estimates for α, m, and μ: $\alpha=3$, [11,12,15] or 1, [10] (see Sec. II B); $m=2,\frac{3}{2}$ or even smaller, as discussed in Sec. II C; and μ of the order 10^{-1} to 1 (see Sec. II B).

Regardless of the particular choice of these parameters, the lamellar (L) phase dominates at sufficiently low temperature, whereas other periodic phases may occur at higher T, in agreement with qualitative considerations at the end of Sec. III A (see Fig. 13). For some choices of the phenomenological parameters, the antiferromagnetic (A) phase intervenes between the bicontinuous (B) and lamellar phases even for ϕ_s as small as a few percent. Similarly the columnar (C) phase may occur at small ϕ_s, but only on the boundary of the aforementioned range for μ ($\mu<0.1$). Therefore, in Fig. 13, we have chosen not to show diagrams with the C phase and to focus on the interesting interplay between the A and L phases.

The four basic types of diagrams in Fig. 13 correspond to the following ranges of parameters: (I) $\mu/m>f(m\alpha)$, $m\alpha<3$; (II) $\mu/m<f(m\alpha), m\alpha<3$; (III) $\mu/m>f(m\alpha), m\alpha>3$; and (IV) $\mu/m<f(m\alpha)$, $m\alpha>3$, where $f(x)$ is a decreasing function of x with $f(2)\approx0.36$ and $f(6)\approx0.22$. In the following we summarize the main features of these diagrams.

For $m\alpha<3$ (type I and type II diagrams), coexistence states between the dilute phase and other phases appear. In particular, there is coexistence between dilute and bicontinuous phases and a middle phase. As $m\alpha\to3$, these coexistence states are depressed towards $\hat{T}=0$, and there is a transition at $m\alpha=3$ to type III and type IV diagrams in which there is a second-order D-B transition and no coexistence of D with other phases (see Fig. 13). Note that, even in type I and type II diagrams the D-B transition is second order at sufficiently high $\hat{T}$. Near the D-B critical line the D phase may itself become "bicontinuous," i.e., it may consist of percolating oil and water domains.[2,4]

An interesting feature of our diagrams is the presence of the antiferromagnetic phase. Its relation to other phases in type I and type III diagrams is different from that in type II and type IV diagrams. In the former types, there is a direct bicontinuous-to-lamellar transition, and the A phase occurs at relatively large values of ϕ_s, while in the latter types, there is a direct bicontinuous-to-antiferromagnetic transition but no direct bicontinuous-to-lamellar transition. The antiferromagnetic phase intervenes between the bicontinuous and lamellar phases in type II and type IV diagrams and occurs at much smaller values of ϕ_s than in type I and

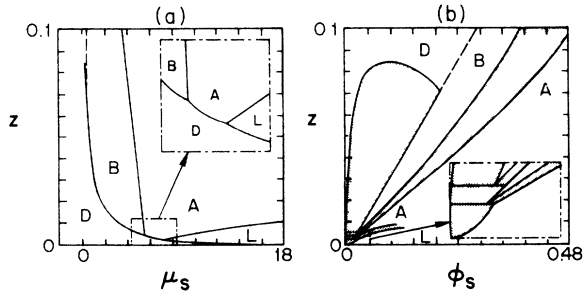

FIG. 15. (a) Type II phase diagram in the (μ_s,z) plane for $m\alpha=2.22$ and $\mu/m=0.34$. The inset gives the region with two triple points. (b) The same in the (ϕ_s,z) plane.

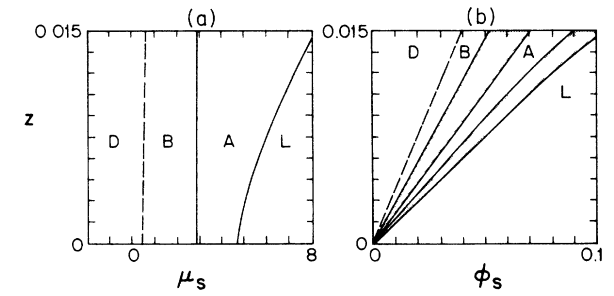

FIG. 17. (a) Type IV phase diagram in the (μ_s,z) plane for $m\alpha=3.18$ and $\mu/m=0.32$. (b) The same in the (ϕ_s,z) plane.

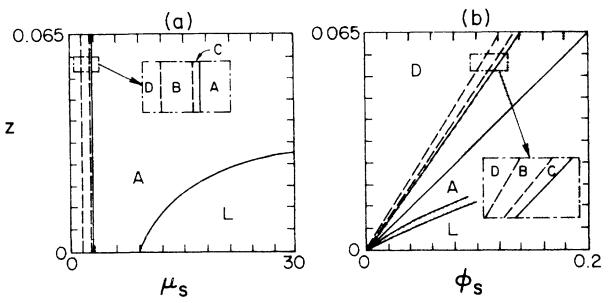

FIG. 18. (a) An example of a (μ_s,z) phase diagram containing the C phase ($m\alpha=6$, $\mu/m=0.1$). (b) The same in the (ϕ_s,z) plane.

type III diagrams (see Fig. 13). In the chemical potential phase diagrams, the antiferromagnetic phase in type II and type IV phase diagrams occurs in the region of ultralow surface tension ($\sigma_s \approx T\xi_p^{-2}$, see Sec. III C), whereas it occurs at relatively higher values of the surface tension in type I and type III diagrams.

When $\mu \gg 1$, i.e., when effects of steric entropy are weak [see Eq. (2.28)], the D-B-L multiple point in type I diagrams appears at high $\hat{T}$ with $\xi \approx \xi_p \approx a$ in the middle phase. However, as μ is decreased to a realistic value of $O(1)$, the temperature of this point is strongly reduced, so that D-B coexistence occurs in a range of $\hat{T}$ with $\xi \approx \xi_p \gg a$ in the middle phase and $\xi \approx a$ in the dilute phase. These properties of the D-B coexistence are consistent with experimental observations. Thus, the effects of steric entropy discussed in this paper are indirectly responsible for the existence of a realistic middle phase microemulsion via the suppression of the lamellar phase.

Structural length scales ξ on either side of the various transition lines in Fig. 13 are typically of order ξ_p. An exception to this rule occurs in type I and type II diagrams in which $\xi \approx a$ in the dilute phase when it coexists with other phases. This is in agreement with Refs. 1–3. In these types of diagrams, there is generally a region of D-D coexistence with a liquid-gas-like critical point, while the D-B critical line terminates at a critical end point (see Fig. 13). At temperatures just below this point, there is three-phase coexistence of the middle phase with dilute phases, whereas at temperatures just above the end point there is a second-order D-B transition and a region of D-D coexistence. In this region a dilute phase, arising itself from a phase separation, further separates into two kinds of dilute phases having different length scales, $\xi \approx a$ and $\xi \approx \xi_p$, respectively. Thus, the D-D coexistence region in Fig. 13 corresponds to four-phase coexistence.

Available experimental data[7,29–32] on balanced systems indicate the existence of direct first-order lamellar-to-bicontinuous and dilute-to-bicontinuous transitions. Thus, they are consistent with type I diagrams. Our model predicts such a diagram within the acceptable range of the phenomenological parameters. Moreover, as explained above, steric entropy plays an important role in determining the properties of a realistic middle phase with a structural length scale $\xi \approx \xi_p \gg a$.

Examples of the above four types of diagrams obtained numerically from mean-field theory of Sec. III numerically are given in Figs. 14–17. An example of a diagram with the columnar phase is given in Fig. 18. In the following we will try to document and explain some of the aforementioned properties of phase diagrams.

B. Nature of the phase transitions

As discussed in Sec. III C, phase transitions between two phases which both have $\xi \approx \xi_p = a/z \gg a$ at the transition occur along an almost vertical straight line in the (μ_s,z) plane (i.e., μ is almost constant along the phase boundary at low z). This is documented in Figs. 14–18 in which many of the transitions are of this kind. If such a transition is first order, then the corresponding coexistence region in the (ϕ_s,z) plane is bounded by two almost straight lines at low z (Figs. 14–18). Phases involved in these transitions have length-scale-dependent free-energy densities $\tilde{\Phi}(N,y)$, Eq. (3.19′), whose minima have a finite limit when $z=a/\xi_p=\exp[-4\pi/(\alpha\hat{T})]\to 0$. These minima occur typically at some $y=O(1)\gg z$ corresponding to $\xi=O(\xi_p)\gg a$. For example, the L-B transition illustrated in Fig. 19 is of this kind.

However, not all of the transitions are of this kind. Exceptions are first-order transitions between D and other phases which occur for $m\alpha<3$, i.e., in type I and type II diagrams (see Figs. 13, 14, and 15). Let us discuss these transitions. From Eq. (3.27), it can be shown that for $z=0$

$$\tilde{\Phi}(D,y)=-y^{m\alpha-3} \tag{4.1a}$$

for $y \ll 1$ or, equivalently,

$$\Phi(D,\xi)=-\frac{T}{\xi_p^3}\left[\frac{\xi}{\xi_p}\right]^{m\alpha-3}, \tag{4.1b}$$

for $\xi \ll \xi_p$. Thus for $m\alpha<3$ and $z=0$, the length-scale-dependent free-energy density of the dilute phase diverges to $-\infty$ when $y=\xi/\xi_p\to 0$. This is consistent with the form of type I and type II diagrams which shows that the D phase always dominates at sufficiently small z in the (μ_s,z) plane (see Figs. 14 and 15). Equations (4.1) are valid for $z \ll y \ll 1$ ($a \ll \xi \ll \xi_p$). For $y \approx z$ ($\xi \approx a$), the divergence of these expressions for $m\alpha<3$ is prevented by the term $(1-z/y)^{-2}=(1-a/\xi)^{-2}$ in the free energy (3.27). Thus, for $m\alpha<3$, ξ minimizing $\Phi(D,\xi)$ is of order a. So, in type I and type II phase diagrams, the

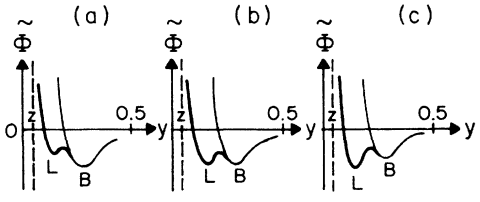

FIG. 19. (a) Length-scale-dependent free-energy densities $\tilde{\Phi}$ of the B (thin curve) and L phases (thick curve) at low temperatures ($z \ll 1$). $y=\xi/\xi_p$ and $z<y<1$. The minima of these curves have a finite limit when $z\to 0$. (a)–(c) represent the situation above, at and below the first-order L-B transition.

structural length scale of the dilute phase is of order of the short distance cutoff a at low temperatures. This results in strong first-order transitions at low temperatures (i.e., small z) between the D phase with $\xi \approx a$ and other phases with $\xi \approx \xi_p \gg a$ (see Figs. 13, 14, and 15). In particular, for $m\alpha < 3$ there is D-B coexistence between the middle phase (B) ($\xi \approx \xi_p \gg a$) and dilute phases (D) consisting of small oil droplets of radius $\xi \approx a$ or, conversely, of small water droplets in oil (see Fig. 20).

In addition to the minimum at $\xi \approx a$, $\Phi(D,\xi)$ may have another minimum at $\xi \approx \xi_p$ [i.e., $\tilde{\Phi}(D,y)$ may have two minima at $y_1 = O(z)$ and $y_2 = O(1)$ as shown in Fig. 21(a)]. The D-D coexistence in type I and type II diagrams is the result of the competition between these two minima [Fig. 21(a)]. The second-order D-B line in type I and type II diagrams is a line of transitions between the minimum of $\Phi(D,\xi)$ at $\xi \approx \xi_p$ and that of $\Phi(B,\xi)$ also at $\xi \approx \xi_p$ [Figs. 21(b)–21(c)]. The corresponding phase boundary is a nearly vertical line in the (μ_s,z) plane.

For $m\alpha > 3$, the functions (4.1) are finite when $y = \xi/\xi_p \to 0$. In fact, for $m\alpha > 3$ (type III and type IV diagrams) $\Phi(D,\xi)$ has only a single minimum at $\xi \approx \xi_p$. The D-B transition in these types is exclusively second order with a nearly vertical phase boundary in the (μ_s,z) plane and $\xi \approx \xi_p$ at the transition (Figs. 16 and 17). Details of this transition are depicted in Fig. 22. As $m\alpha \to 3$ from below, first-order boundaries between D and other phases in type I and type II diagrams are depressed to zero temperature (i.e., $z = 0$). Thus, to summarize, coexistence of D with other phases (in particular, with the middle phase) may occur only for $m\alpha < 3$ (type I and type II diagrams).

We now discuss transitions other than those in which the D phase is involved. They are all first order (except at some isolated points on the L-A phase boundary in types I and III as in Figs. 13, 14, and 16). Typical structural length scales ξ are of order ξ_p at the B-A and B-L transition (See Fig. 19). The corresponding phase boundaries are almost vertical in the (μ_s,z) plane at small z, i.e., at low $\hat{T}$ (when $\xi \approx \xi_p = a/z = a \exp[4\pi/(\alpha\hat{T})] \gg a$), in agreement with remarks given at the beginning of this section. The physical picture of the B-L melting which occurs when the interlamellar spacing ξ reaches some distance of the order ξ_p was already anticipated in Sec. II B. When it occurs at low z, the L-A transition is of the same nature, with $\xi \approx \xi_p$ in both phases at the transition. Thus, to summarize, all structural length scales ξ at all transitions occurring at low $\hat{T}$ (i.e. small z) are of order ξ_p, except in the D phase of type I and type II diagrams in which $\xi \approx a \ll \xi_p$ at coexistence with other phases.

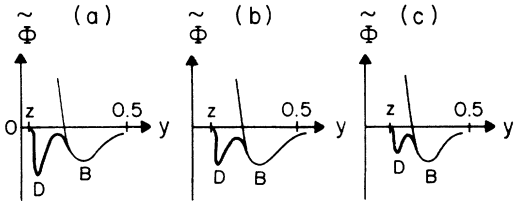

FIG. 20. Length-scale-dependent free-energy densities $\tilde{\Phi}$ of D and B phases (thick and thin curves, respectively) for $m\alpha < 3$. At low T ($z \ll 1$), the D curve has a minimum at $y = 0(z)$. (a)–(c) represent situations below, at, and above the first-order D-B transition. For $y > > z$ the shapes of these curves are nearly z independent. μ_s is taken to be a constant while z increases from (a) to (c).

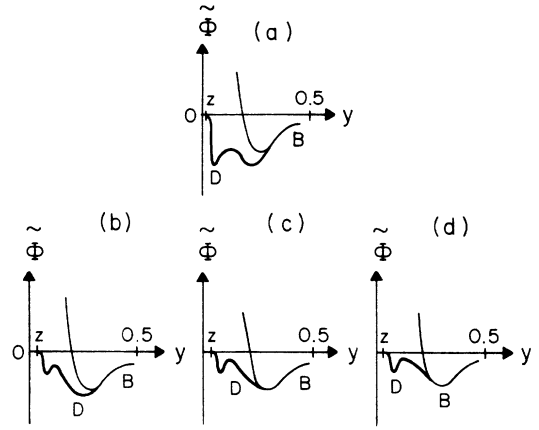

FIG. 21. (a) Length-scale-dependent free-energy densities $\tilde{\Phi}$ of the D and B phases at $D-D$ coexistence, $m\alpha < 3$. The D curve (thick) has two minima at $y = 0(z)$ and at $y = 0(1)$. (b)–(d) represent, respectively, situations below, at, and above the second order D-B transition. μ_s increases from (b) to (c).

An interesting aspect of the phase diagrams we have calculated numerically is their dependence on the strength of steric entropy, which is inversely proportional to μ [see Eq. (2.28)]. Thus, for $\mu/m > f(m\alpha)$, type I and type III diagrams occur with a direct B-L transition (see Figs. 13, 14, and 16), while for $\mu/m < f(m\alpha)$, type II and type IV diagrams occur in which there is no such transition since the A phase intervenes between the B and L phases (see Figs. 13, 15, and 17). At smaller, presumably unrealistic values of μ ($\mu < 0.1$ or even smaller), there may appear some new types of diagrams containing the C phase in the region of a small surfactant concentration (of the order of a few percent) characterized by $\xi \approx \xi_p$ and low interfacial tension of order $T\xi_p^{-2}$ at low temperatures. Figure 18 gives a numerical example of such a diagram.

An important feature related to the steric entropy is its

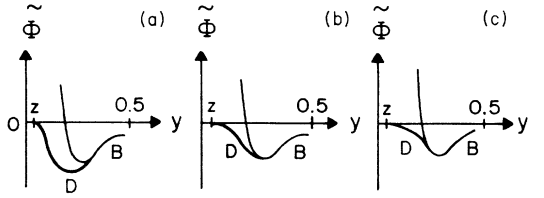

FIG. 22. Length-scale-dependent free-energy densities $\tilde{\Phi}$ of the D and B phase for $m\alpha < 3$ (thick and thin curves, respectively). (a)–(c) represent, respectively, situations below, at, and above the second-order D-B transition.

influence on the typical length scale ξ in the middle phase at D-B coexistence which occurs for $m\alpha<3$ (type I and type II diagrams). Within this theory, this length scale is of the order $\xi_p=a/z=a\exp[4\pi/(\alpha\hat{T})]$. Experimentally, ξ is typically a few hundred angstroms—much larger than the molecular length scale a. In type I diagrams (Figs. 13 and 14), whose form is consistent with experimental observation, D-B coexistence occurs in the temperature range between the end point of the D-B critical line and the D-B-L multiple point. In order to achieve a realistic middle phase with $\xi\approx\xi_p=a/z\gg a$, this temperature range should occur at low $\hat{T}$, i.e., small z. Thus it is favorable to have the D-B-L multiple point at some small z. This is realized, for example, in the type I diagram at $m\alpha=2.64$ and $\mu/m=0.38$ (Fig. 14) in which the D-B-L multiple point is at $z=0.000\,25$ with

$$\xi/\xi_p=0.38\ ,\quad \phi_s=0.001\ ,\quad a/\xi=0.0007 \tag{4.2a}$$

in the middle phase. On the other hand, when μ is unrealistically large (i.e., when the effects of steric entropy are small) the D-B-L multiple point occurs in the region of relatively high $\hat{T}$ and large z. For example, for the case $m\alpha=2.64$, $\mu/m=2.8$, the multiple point occurs at $z=0.018$ with

$$\xi/\xi_p=0.44\ ,\quad \phi_s=0.06\ ,\quad a/\xi=0.04 \tag{4.2b}$$

in the middle phase. The corresponding numbers for the case $m\alpha=2.64$ and $\mu/m=28$ are $z=0.075$ and

$$\xi/\xi_p=0.48\ ,\quad \phi_s=0.26\ ,\quad a/\xi=0.16\ . \tag{4.2c}$$

Thus the steric entropy with magnitude proportional to $1/\mu$ [see Eq. (2.28)] plays an important role in explaining the properties of the middle phase. A realistic value of μ of order unity or smaller may ensure the existence of a realistic middle phase with a structural length scale which is, say, hundreds or even thousands times larger than the microscopic length scale a.

C. Comparison with experiments

As already mentioned, type I diagrams (see Figs. 12 and 14) are consistent with the experiments on microemulsions[29–32] and analogous surfactant systems,[7] which indicate the existence of direct first-order transitions from lamellar-to-bicontinuous and from bicontinuous-to-dilute phases. Trends depicted in Fig. 14 are indeed in agreement with the data of Kahlweit and co-workers[29–32] on the micoremulsions with a 1:1 oil-to-water volume ratio taken along balanced lines.[33] Just as in the diagram of Fig. 14, these experiments indicate a lamellar-to-bicontinuous phase first-order line with surfactant concentration $\phi_{s1}(z)$ in the bicontinuous phase and a bicontinuous-to-dilute phase first-order line with some $\phi_{s2}(z)$ in the bicontinuous phase (i.e., in the middle phase). These lines meet at a lamellar-bicontinuous-dilute phase multiple point where $\phi_{s1}(z)=\phi_{s2}(z)\equiv\phi_{s,\min}$. In these experiments, the parameter $z=\exp[-4\pi K_M(a)/(\alpha T)]$ is varied by varying the surfactant chain length[33] as depicted in Figs. 3 and 6 of Ref. 30. Thus, for a surfactant with a short chain length and thus a small bare membrane rigidity $K_M(a)$, the bicontinuous phase exists in a broad range of surfactant concentrations $\phi_{s2}(z)<\phi_s<\phi_{s1}(z)$. Upon increasing the surfactant chain length and thus increasing $K_M(a)$, i.e., decreasing z, this range for ϕ_s vanishes at a lamellar-bicontinuous-dilute phase multiple point, as it does in Fig. 14. For still longer surfactant chain lengths, there is only coexistence between lamellar and dilute phases, just as in Fig. 14. Moreover, experimentally, both $\phi_{s1}(z)$ and $\phi_{s2}(z)$ are *increasing* functions of a for z above the multiple point for which $\phi_{s1}(z)=\phi_{s2}(z)=\phi_{s,\min}$, in agreement with Fig. 14. The surfactant concentration $\phi_{s,\min}$ in the bicontinuous phase at the lamellar-bicontinuous-dilute phase multiple point is the smallest concentration with which one can obtain the random bicontinuous phase (see Fig. 14). Since the cost of any commercial microemulsion is directly proportional to the amount of surfactant needed to make it, the cheapest bicontinuous microemulsions are those with $\phi_s\gtrsim\phi_{s,\min}$ and a 1:1 oil-to-water volume ratio. At the end of Sec. IV B, we demonstrated that typically small values of $\phi_{s,\min}$ are an effect of steric entropy which suppresses the lamellar-bicontinuous-dilute phase multiple point to low values of ϕ_s and z. An unrealistically small value of $1/\mu$ yields a large $\phi_{s,\min}$, as in Eq. (4.2c), while a realistic $1/\mu=O(1)$ yields a realistic $\phi_{s,\min}=O(1\%)$ as in Eq. (4.2a). Thus, the possibility of having reasonably priced microemulsions is in a sense the result of the effects of steric entropy. In the absence of these effects, the price would be more than a hundred times larger, as can be seen by comparing Eqs. (4.2a) and (4.2c).

Throughout our discussion, we have considered α, m, and μ as phenomenological parameters and have studied the sensitivity of phase diagrams to their values. These values are largely uncertain, as explained in Sec. II. The actual value of the product $m\alpha$ is of importance for understanding why the coexistence regions of dilute with other phases exist in reality. We found that these regions are present only for $m\alpha<3$ (see Fig. 12). In the following, we present a simple and crude argument for a particular $m\alpha<3$. Consider a spherical oil droplet of radius ξ immersed in a water background. Within the framework of our approach, its bending energy is given by Eq. (2.48). On the other hand, from Eqs. (2.23) and (2.24) this energy is

$$8\pi K_M(\xi)+4\pi K_G(\xi)=(2\alpha-\alpha')\ln(\xi_p/\xi)\ .$$

By matching this equation to Eq. (2.48) and using $\alpha=3$ and $\alpha'=\frac{10}{3}$ (see Sec. II B), one obtains

$$m\alpha=2\alpha-\alpha'=8/3\ <\ 3\ ,$$

which ensures the existence of first-order transitions between dilute and other phases. The above argument is interesting from another point of view. The model proposed here is a single bending constant approximation since Eq. (2.36) is postulated. On the other hand, the ap-

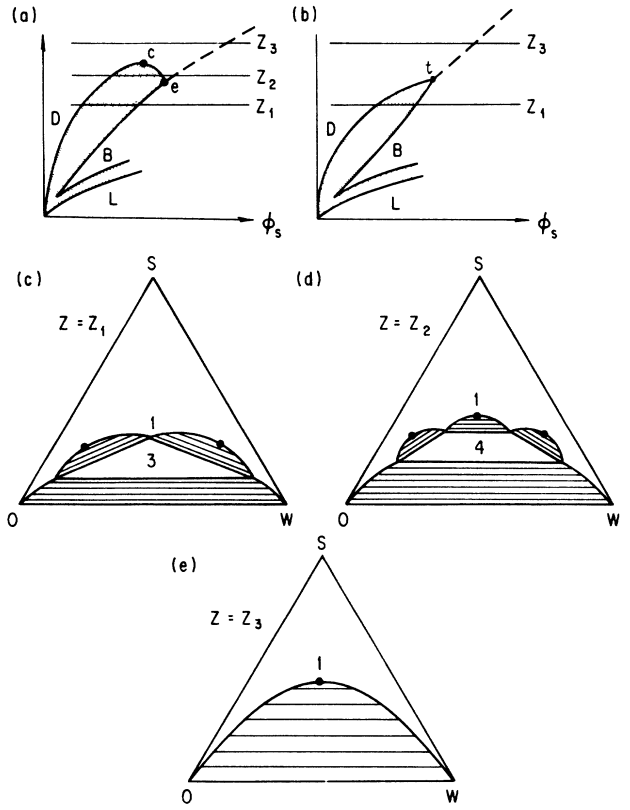

FIG. 23. (a) Schematic representation of a typical type I phase diagram of balanced microemulsion at equal volume of oil and water. It has a region of four-phase coexistence between the critical end point e and the critical point c. An alternative to (a) is the diagram shown in (b) with a tricritical point t. (c)–(e) give schematic ternary oil-water-surfactant phase diagrams corresponding to values $z=z_1$, z_2, and z_3 which are indicated in (a) and (b). For simplicity, we depict only equilibria between uniform phases. Two-phase equilibria are indicated by tie lines, while one-, three-, and four-phase regions are indicated with numbers 1, 3, and 4. Various critical points are indicated by dots.

proach used above to derive a realistic estimate $m\alpha=\frac{8}{3}$ indicates that it might be possible to account for the effects of nonzero Gaussian curvature rigidity by making a suitable choice for the parameter $m\alpha$ entering our single bending constant model.

We now proceed to discuss in more detail the phase equilibria between uniform phases. We recall that these phases are the ferromagnetic and paramagnetic phases of the model. Three typical situations are depicted in Fig. 23. At small z (i.e., large reduced rigidity), e.g., $z=z_1$ in Figs. 23(a) and 23(c), one has regions of two- and three-phase coexistence of the type that have been discussed previously.[1] There are two critical points which occur at two phase coexistence regions. At a larger z, e.g., $z=z_3$ in Figs. 23(a) and 23(e) there is simple two-phase coexistence with a single critical point, entirely analogous to that occurring in the standard Ising ferromagnet. Both kinds of phase behavior obtained from the theory have been observed by Kahlweit and co-workers.[29,30] However, these experiments have not observed behavior such as that at $z=z_2$ in Figs. 23(a) and 23(d) in which there is four-phase coexistence among four ferromagnetic phases: two oil-rich phases characterized by different structural length scales and surfactant volume fractions (see Sec. IV B) and two water-rich phases related to the oil-rich phases by the oil-water, i.e., by the Ising up-down, symmetry. The experiments of Refs. 29 and 30 on ternary oil-water-surfactant systems, as well as microscopic models of microemulsions, suggest the possibility of a simpler scenario, depicted in Fig. 23(b), for interpolating between Figs. 23(c) and 23(e). There, a standard tricritical point (t) joins the coexistence loop and the second order line between the ferromagnetic and the paramagnetic phases. However, experiments of Bennet, Davix, and Scriven[34] on quasiquaternary systems, as well as some results of Kahlweit and Strey (see Ref. 31, Sec. VI), are consistent with the scenario in which a narrow four-phase region occurs. These two scenarios in Figs. 23(a) and 23(b) can be joined in a continuous manner. The critical point c and the critical end point e can merge continuously into a single tricritical point t and the region of four-phase coexistence shrunk to zero as a function of some control parameter.[35] We have found that this four-phase region can be made smaller by choosing smaller values of $m\alpha$ than those used in calculating diagrams in Figs. 14–18. Then one can produce phase diagrams with a very small region of four-phase coexistence and thus approximating very closely a tricritical point. An example of a phase diagram with this close to tricritical behavior was calculated in Ref. 2 (see Fig. 2 of Ref. 2). There the value of $m\alpha=2$ was used and steric entropy effects were neglected. Steric entropy only weakly influences the free energy of the dilute (ferromagnetic) phase and phase equilibria between uniform phases, as discussed in Sec. V in more detail.

Four-phase regions were studied experimentally by Bennet, Davix, and Scriven in quasiquaternary systems with oil, brine, surfactant, and alcohol (cosurfactant) as components.[34] Our model, however, describes ternary or quasiternary systems. Thus, the four-phase region appears as a trapezoid in the ternary phase diagrams [see Fig. 23(d)]. For a quaternary system, this region is a tetrahedron in the quaternary phase diagram. Experiments,[34] however, typically indicate narrow four-phase regions and a four-phase tetrahedron which is almost degenerate, i.e., nearly planar, and can be described approximately as a trapezoid in Fig. 23(d). Thus the quasiternary description could be appropriate, and four-phase coexistence regions observed in experiments could be related to those obtained from our model. It is interesting to note that the model predicts four-phase regions to occur even in truly ternary systems. For these systems, volume fractions of phases in the four-phase region are not uniquely determined by the position of the mixing point within the four-phase trapeziod (since the number of phases, 4, exceeds the number of components, 3, by 1). In practice, these volume fractions would be fixed by small amounts of impurities, which are components in addition to the three dominant ones. This might make the observation of the four-phase region in an approxi-

mately ternary system difficult. Experimentally, the behavior observed in ternary systems is interpreted as tricritical,[29,30] as in Fig. 23(b). We believe that the existence of a four-phase region even in these systems cannot be excluded. As discussed in the preceding paragraph, the four-phase region can be small (e.g., for $m\alpha \leq 2$), and the overall behavior might only resemble that of a tricritical point. Moreover, relative volume fractions in the four-phase region might be strongly influenced by small amounts of impurities, which might further complicate the observation of a four-phase region in practice. Four-phase regions are more easily observed in quaternary systems[34] in which the amount of the fourth component is not small. To understand fully these realistic four-phase regions, one needs further extensions of the present theory which explicitly account for the presence of the fourth component in quaternary systems (e.g., cosurfactant) or for the effects of small amounts of impurities in a nearly ternary system.

An interesting theoretical finding of our work is that periodic "antiferromagnetic" and columnar phases in addition to the lamellar phase may appear in systems with a 1:1 oil-to-water volume ratio as shown in Fig. 13. In the realistic type I diagram (see Figs. 13 and 14), this occurs in the same range of surfactant concentration ϕ_s in which the lamellar phase occurs, but at larger values of z, i.e., at smaller values of the reduced rigidity $K_M(a)/T$, for physical reasons discussed at the end of Sec. III A. An experimental check of this result is, in principle, possible, e.g., in the systems studied in Ref. 30, by adding cosurfactant and thus decreasing the rigidity below the values already studied.

Finally, we stress that the model developed here is appropriate to the random surface systems with short-range repulsion, e.g., for nonionic surfactant monolayer or bilayer systems. Systems with unscreened Coulomb interactions, which dominate over the Helfrich entropic repulsion, can have a significantly different phase behavior (see, e.g., Ref. 16). If the electrostatic interaction is screened by adding brine, the screening length may be taken as the microscopic short-distance cutoff of the present theory, and the phase behavior could be traced by using the results of the present work. In fact, experimental results of Safinya and Roux, Ref. 16, support this idea. It would be interesting to study this problem in more detail.

V. SUMMARY AND DISCUSSION

We constructed a simple coarse-grained model for microemulsions which is a qualitative improvement with respect to previous phenomenological models[1–3,9] of Talman and Prager, de Gennes and co-workers, Widom, and more recently of Safran and co-workers. We demonstrated here that there is necessarily an entropic contribution, missing in all previous theories, to the coarse-grained free energy whose origin is the same as that of Helfrich's entropic repulsion[14–18] stabilizing lamellar multimembrane phases. The inclusion of this steric entropy in the previous phenomenological studies is essential if they are to be used in the study of periodic phases in microemulsions and analogous surfactant systems. Thus our model enables us to obtain the global phase diagram containing both uniform and periodic phases of microemulsions and analogous surfactant systems.[7,29,32] This is a significant improvement with respect to previous phenomenological studies which were applied consistently only to uniform phases.

We demonstrated also that inclusion of steric entropy is essential to explain the existence of the middle phase microemulsion with a structural length scale ξ much larger than the molecular scale a. In the absence of periodic phases, one may have such a middle phase even in the absence of steric entropy [i.e., if μ in Eq. (2.28) is infinite]. However, once the periodic phases are included in the theory, the temperature range and, consequently, the value of ξ in the middle phase are limited by the presence of the coexistence regions of the dilute with periodic phases. We have shown that steric entropy of a realistic magnitude may suppress these regions to sufficiently low temperatures and thus that ξ is necessarily much greater than a in the middle phase.

Within the phenomenological approach, steric entropy is generated naturally by coarse graining. For $\xi \approx \xi_p$ its effect is quantitatively comparable to the effects of entropy of mixing and bending rigidity considered in Refs. 1–3. The simple formula we use to include steric entropy, Eq. (2.28), underestimates somewhat its magnitude when $\xi \ll \xi_p$, while it is qualitatively correct when $\xi \lesssim \xi_p$. To see this, consider, e.g., fluctuations around the mean surface configuration corresponding to the presence of a passage in the lamellar phase (Fig. 5). The entropy decrease due to steric effects is in general[18] of the order L_1^{-2} per unit area. The average distance, L_1, between collisions of the membrane with fictitious hard walls is related to ξ by Eq. (2.18) only for straight sections of the lamellar phase which are far from the passage. On the other hand, in the region of the passage, we expect $L_1 \approx \xi$ rather than $L_1 \approx \xi[K_M(L_1)/T]^{1/2}$ as given by Eq. (2.18). The condition $\xi \approx L_1 \approx \xi_p$ which implies $K_M(L_1) \approx T$, is fulfilled at various phase transitions that we find in Sec. IV so that the use of Eq. (2.28) is qualitatively correct. In general, use of Eq. (2.28) underestimates steric entropy when mean interfaces are heavily curved and $\xi \ll \xi_p$ [so that $K_M(L_1) \gg T$]. However, in these cases, the contribution of the steric entropy is subdominant to that of bending rigidity. Thus, our way of including steric entropy via Eq. (2.28) is a reasonable one if one wants to consider phase equilibria.

Within our theory, the structural length scale ξ is determined by the variational principle Eq. (2.15). When the equilibrium state is a perfectly ordered lamellar phase, this variational principle reduces to that of a recent theory[15] for steric stabilization of lamellar systems. Here, the concept of steric entropy is extended to states which could be far from any ordered structure. ξ is typically of the order ξ_p at a variety of phase transitions, except in dilute phases coexisting with other phases (e.g., the middle phase) in type I and type II diagrams when $\xi \approx a \ll \xi_p$. In fact, the existence of these coexistence regions crucially depends on this property of dilute phases which is realized if $m\alpha < 3$ (see Sec. IV). An interesting generalization of our theory would be to allow for spatial

fluctuations of ξ around the variationally determined length scale. This may give some insight into polydispersivity effects which were recently addressed by Huse and Leibler in Ref. 4.

Let us compare the present theory with previous phenomenological studies of Safran and co-workers.[1-3]. The most significant difference is that we have included the effects of steric entropy whereas the previous studies did not. This enabled us to study phase equilibria involving periodic as well as spatially uniform phases. Steric entropy, however, has only a weak quantitative effect on the free energy of the dilute phases of the model when they coexist with other phases. In this case, the steric term of the model only provides a short-distance cutoff to ξ of order a. For $a<\xi\ll\xi_p$, the steric entropy contribution to the free energy of the dilute phase is subdominant to that of the bending term. Thus, our estimate for this free energy is basically the same as that of the model of Refs. 1–3. As a consequence, all aspects of phase equilibria involving the dilute phase discussed in Sec. IV [e.g., the different nature of transitions for $m\alpha>3$ and $m\alpha<3$, the validity of Eq. (4.1), the appearance of four-phase coexistence, etc.] are common features of our model and that of Refs. 1–3. However, only a particular value of $m\alpha$ ($m\alpha=2$) was considered in Refs. 1–3.

Finally, let us stress that our study, as well as previous ones,[1-3] employs a single bending constant approximation, i.e., Eq. (2.36) is presumed. Thus, possible interesting effects associated with the Gaussian curvature bending constant K_G are neglected.[25] Positive K_G favors creation of passages[4] or a fusion of a number of surfaces into a smaller number of bigger ones as in Fig. 6.[4] Thus, for example, we interpreted our antiferromagnetic phase as a crystal of oil droplets immersed in water background and vice versa. Positive K_G may favor creation of passages connecting neighboring droplets, thus transforming the droplet crystal into a crystal-like phase made of a single extensive surface.[4] A further geometrical refinement of the theory would be necessary to include some of the realistic such phases[4] in the phenomenological treatment.

ACKNOWLEDGMENTS

We thank M.E. Cates, D. Roux, S.A. Safran, and M. Schick for discussions and the Aspen Center for Physics where a part of this work was carried out. This work was supported in part by the Laboratory for Research on the Structure of Matter under National Science Foundation Grant No. DMR85-195909 and by National Science Foundation Grant No. DMR85-20272. L.G. acknowledges support by the U.S. Department of Energy, under Grant No. DE-FG 03-88 ER 45378.

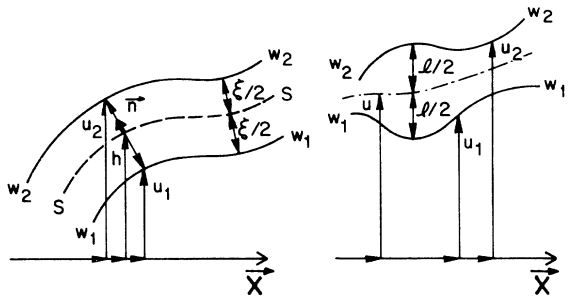

FIG. 24. Hard wall configurations discussed in the Appendix.

APPENDIX

Here we discuss the relationship between some results of Ref. 15 and Eq. (2.17) which gives the free energy of a fluid membrane constrained by two hard walls w^1 and w^2 separated by a constant distance ξ as in Figs. 7 and 23(a), to fluctuate around the mean surface $\mathbf{R}_0(\mathbf{x})$ (Fig. 24). Let us presume that the mean surface is nearly planar and satisfies periodic boundary conditions [in this case the Gaussian curvature term of (2.17) does not contribute], and let us parametrize the surface by means of the height $h(\mathbf{x})$ above a base plane with Euclidean coordinates $\mathbf{x}$, i.e., $\mathbf{R}_0=(\mathbf{x},h(\mathbf{x}))$. Then (2.17) gives

$$f(\xi,h(\cdots))=\int d^2x\{a(L_1)[1+\tfrac{1}{2}(\nabla h)^2] +\tfrac{1}{2}K_M(L_1)(\nabla^2 h)^2+\cdots\}\ . \tag{A1}$$

The ellipses in (A1) indicate higher-order terms in $h(\mathbf{x})$. However, from (A1) it is clear that to determine $A(L_1)$ and $K_M(L_1)$, it suffices to calculate $f(\xi,h(\cdots))$ to quadratic order in $h(\mathbf{x})$.

On the other hand, Ref. 15 considers a more general problem of a surface fluctuating around the mean surface with height function $u(\mathbf{x})$ between two hard walls defined by height functions

$$u_1(\mathbf{x})=u(\mathbf{x})-l(\mathbf{x})/2\ ,\quad u_2(\mathbf{x})=u(\mathbf{x})+l(\mathbf{x})/2\ , \tag{A2}$$

as depicted in Fig. 23(b). When $l(\mathbf{x})$ varies slowly around some value l,

$$l(\mathbf{x})=l+\delta l(\mathbf{x})\ , \tag{A3}$$

one can expand the free energy of the surface in powers of $\delta l(\mathbf{x})$ and $u(\mathbf{x})$[15],

$$f[l+\delta l(\cdots),u(\cdots)]=\int d^2x\{a_0(l)+a_1(l)\delta l(\mathbf{x})+\tfrac{1}{2}a_2(l)[\delta l(\mathbf{x})]^2+\tfrac{1}{2}b(l)[\nabla u(\mathbf{x})]^2+\tfrac{1}{2}K(l)[\nabla^2 u(\mathbf{x})]^2+\cdots\}\ , \tag{A4}$$

with

$$a_k(l)=\frac{\partial^k a_0(l)}{\partial l^k}\ . \tag{A5}$$

Rotational invariance imposes the following relation between $b(l)$ and $a_0(l)$:[15]

$$b(l)=-l^2\frac{\partial}{\partial l}\left[\frac{a_0(l)}{l}\right]\ . \tag{A6}$$

Now we proceed to relate (A4) to (A1). Note that $l(\mathbf{x})$ in Eq. (A2) is the distance between hard walls measured along direction 3, i.e., perpendicularly to the base plane in Fig. 23. Thus, the situation with $l(\mathbf{x})=$ const [i.e., $\delta l(\mathbf{x})=0$] does not correspond to the present problem, with constant distance between hard walls measured perpendicularly with respect to the mean surface $[\mathbf{x},h(\mathbf{x})]$ as depicted in Fig. 23(a). Related to this is the fact that Eq. (A4), with $\delta l(\mathbf{x})=0$, $l=\xi$, and $u(\mathbf{x})=h(\mathbf{x})$, is not isomorphic to (A1), as can be easily shown by means of (A6). Nevertheless, one can express configurations of the walls in terms of $h(\mathbf{x})$ and ξ by using the following equations following from Fig. 23(a):

$$\begin{aligned} u_1(\mathbf{x}-\mathbf{n}_\perp(\mathbf{x})\xi/2)&=h(\mathbf{x})-n_\parallel(\mathbf{x})\xi/2\ , \\ u_2(\mathbf{x}+\mathbf{n}_\perp(\mathbf{x})\xi/2)&=h(\mathbf{x})+n_\parallel(\mathbf{x})\xi/2\ , \end{aligned} \tag{A7}$$

with $\mathbf{n}=(\mathbf{n}_\perp,n_\parallel)$, the unit normal to the point $(\mathbf{x},h(\mathbf{x}))$ of the mean surface:

$$\begin{aligned} \mathbf{n}(x)&=(\mathbf{n}_\perp(\mathbf{x}),\ n_\parallel(\mathbf{x})) \\ &=(-\nabla h(x),1)\{1+[\nabla h(\mathbf{x})]^2\}^{-1/2}\ . \end{aligned} \tag{A8}$$

From (A7) and (A8) one can find $u_{1,2}$ as functions of $\mathbf{x}$ by an expansion in powers of $h(\mathbf{x})$. For our purpose it is sufficient to keep terms which are $O(h^2)$ at most. Straightforward calculation yields

$$\begin{aligned} u_1(\mathbf{x})&=h(\mathbf{x})-\tfrac{1}{2}\xi\{1+\tfrac{1}{2}[\nabla h(\mathbf{x})]^2\}+\cdots\ , \\ u_2(\mathbf{x})&=h(\mathbf{x})+\tfrac{1}{2}\xi\{1+\tfrac{1}{2}[\nabla h(\mathbf{x})]^2\}+\cdots\ . \end{aligned} \tag{A9}$$

By (A9) and (A2)

$$u(\mathbf{x})=\tfrac{1}{2}[u_1(\mathbf{x})+u_2(\mathbf{x})]=h(\mathbf{x})+\cdots\ , \tag{A10}$$

$$l(\mathbf{x})=u_2(\mathbf{x})-u_1(\mathbf{x})=\xi\{1+\tfrac{1}{2}[\nabla h(\mathbf{x})]^2\}+\cdots \tag{A11}$$

where the ellipses indicate terms which are $O(h^4)$. Thus, by (A11) and (A3) one has

$$\delta l(\mathbf{x})=\tfrac{1}{2}\xi[\nabla h(\mathbf{x})]^2+\cdots \tag{A12}$$

and

$$l=\xi\ . \tag{A13}$$

Introducing $u(\mathbf{x})$, $\delta l(xv)$, and l as in Eqs. (A10), (A12), and (A13) into the free energy (A4) and using (A5) and the Ward identity (A6), one obtains

$$\begin{aligned} &f(l+\delta l(\cdots),u(\cdots)) \\ &\quad=\int d^2x(a_0(\xi)\{+\tfrac{1}{2}[\nabla h(\mathbf{x})]^2\} \\ &\qquad+\tfrac{1}{2}K(\xi)[\nabla^2 h(x)]^2+\cdots)\ . \end{aligned} \tag{A14}$$

Equation (A14) is isomorphic to (A1) with

$$a(L_1)=a_0(\xi), \tag{A15}$$

$$K_M(L_1)=K(\xi)\ . \tag{A16}$$

Equations (A15) and (A16) express the parameters $a(L_1)$ and $K_M(L_1)$ of Eq. (2.17) in terms of the parameters $a_0(\xi)$ and $K(\xi)$ of Eq. (A4) studied in Ref. 15. Detailed expressions for $a_0(\xi)$ and $K(\xi)$ are obtained in the framework of a low-temperature theory in Ref. 15, and the final form of $a(L_1)$ and $K_M(L_1)$ obtained from these expressions and Eqs. (A15) and (A16) is the one presented in Sec. II B. There we explained the physical origin of these parameters.

[1]S.A. Safran, D. Roux, M.E. Cates, and D. Andelman, Phys. Rev. Lett. **57**, 491 (1986); J. Chem. Phys. **87**, 7229 (1987).

[2]M.E. Cates, D. Roux, D. Andelman, S.T. Milner, and S.A. Safran, Europhys. Lett. **5**, 733 (1988).

[3]S.T. Milner, S.A. Safran, D. Andelman, M.E. Cates, and D. Roux, J. Phys. (Paris) **49**, 1065 (1988).

[4]D.A. Huse and S. Leibler, J. Phys. (Paris) **49**, 605 (1988).

[5]For a general survey, see *Physics of Complex and Supermolecular Fluids*, edited by S.A. Safran and N.A. Clark (Wiley, New York, 1987).

[6]See, e.g., J. Meunier, J. Phys. (Paris) Lett. **49**, L-1005 (1985).

[7]Reference 2 contains a survey of recent experimental studies of surfactant bilayer systems dissolved in a single solvent. See also D. Roux and C.M. Knobler, Phys. Rev. Lett. **60**, 373 (1988).

[8]P. Ekwald, in *Advances in Liquid Crystals I*, edited by G.H. Brown (Academic, New York, 1975), p. 1; A.M. Bellocq and D. Roux, in *Microemulsions*, edited by S. Friberg and P. Bothorel (Chemical Rubber, New York, 1986); D.H. Smith, J. Colloid. Interface Sci. **102**, 1241 (1982); B. Widom, J. Chem. Phys. **81**, 1030 (1984).

[9]The phenomenological approach to thermodynamics of microemulsions was initiated by Y. Talmon and S. Prager, J. Chem. Phys. **69**, 2984 (1978); **76**, 1535 (1982); and further developed by J. Jouffroy, P. Levinson, and P.G. de Gennes, J. Phys. (Paris) **43**, 1241 (1982); and B. Widom, J. Chem. Phys. **81**, 1030 (1984).

[10]W. Helfrich, J. Phys. (Paris) **46**, 1263 (1985); **48**, 285 (1987).

[11]L. Peliti and S. Leibler, Phys. Rev. Lett. **54**, 1690 (1985).

[12]D. Forster, Phys. Lett. **114A**, 115 (1986); H. Kleinert, *ibid.* **114A**, 263 (1986); **116A**, 57 (1986).

[13]P.G. de Gennes and C. Taupin, J. Phys. Chem. **86**, 2294 (1982).

[14]W. Helfrich, Z. Naturforsch. **33A**, 305 (1978). Helfrich proposed several estimates for μ.

[15]L. Golubovic´and T.C. Lubensky, Phys. Rev. B **39**, 12 110 (1989).

[16]C.R. Safinya *et al.*, Phys. Rev. Lett. **57**, 2118 (1986). See also D. Roux and C.R. Safinya, J. Phys. (Paris) **49**, 307 (1988); and F.C. Larche *et al.*, Phys. Rev. Lett. **56**, 1700 (1986).

[17]D. Sornette, Europhys. Lett. **2**, 715 (1986).

[18]See, e.g., V.L. Pokrovsky, A.L. Talapov, and P. Bak, in *Solitons*, edited by S.E. Trulinger, V.E. Zakharov, and V.L. Pokrovsky (Elsevier Science, New York, 1986), p. 71; M.E.

Fisher and D.S. Fisher, Phys. Rev. B **25**, 3192 (1982); F.D.M. Haldane and J. Villain, J. Phys. (Paris) **42**, 1673 (1982).

[19]See, e.g., B. Dubrovin, A. Fomenko, and S. Novikov, *Modern Geometry Methods and Applications* (Springer-Verlag, New York, 1987), Vol. 1. A surface embedded in three-dimensional space can be specified by a three-dimensional vector field $\mathbf{R}(\mathbf{x})$, which is a function of a two-dimensional coordinate parametrizing the points on the surface. The geometry of a surface is reparametrization invariant, i.e., invariant with respect to $\mathbf{x}\rightarrow\mathbf{y}(\mathbf{x})$, where $\mathbf{y}(\mathbf{x})$ is an arbitrary invertible two-dimensional mapping.

[20]K. Fujikawa, Phys. Rev. D **23**, 2262 (1981).

[21]Real membranes are allowed to merge or divide into smaller ones. The requirement of the strict, hard-core self-avoidance is in fact imposed to ensure that the trace operator $\mathrm{Tr}_{\{R_j\}}$ is well defined sum over sectors with fixed numbers of surfaces.

[22]W. Helfrich, Z. Naturforsch. **30C**, 841 (1975). See also, W. Helfrich and R.M. Servus, Nuovo Cimento **3**, 137 (1984).

[23]W. Harbich, R.M. Servus, and W. Helfrich, Z. Naturforsch. **33A**, 1013 (1978).

[24]L.D. Landau and E.M. Lifshitz, *Statistical Physics* (Pergamon, Oxford, 1969). We stress that $-\sigma$ is simply a chemical potential coupled to the extensive membrane area equivalent to the surfactant chemical potential of Ref. 1. This quantity should not be confused with the surface tension of the interfaces between coexisting bulk phases at first-order phase transitions between them.

[25]See Ref. 4 for a discussion of possible effects of the Gaussian curvature bending energy. See also, T. Hofsäss and H. Kleinert, J. Chem. Phys. **86**, 3565 (1987).

[26]Note that the value of $B_G(\{\phi_i\})$ is independent of the details smoothing process, since the Gaussian bending rigidity energy is a topological invariant. See Ref. 25.

[27]M. Schick and W.H. Shih, Phys. Rev. Lett. **59**, 1205 (1987); G. Gomper and M. Schick, *ibid.* **62**, 1647 (1988). A different lattice model is considered in K. Chen, C. Ebner, C. Jayaprakash, and R. Pandit, J. Phys. C **20**, L361 (1987); and Phys. Rev. A **38**, 6240 (1988).

[28]See, e.g., R.P. Feynman, *Statistical Mechanics* (Addision Wesley, Reading, MA, 1972).

[29]M. Kahlweit, R. Strey, and D. Hasse, J. Phys. Chem. **89**, 163 (1985).

[30]M. Kahlweit, R. Strey, and P. Firman, J. Phys. Chem. **90**, 5239 (1986).

[31]M. Kahlweit and R. Strey, J. Phys. Chem. **91**, 1553 (1987).

[32]M. Kahlweit and R. Strey, J. Phys. Chem. **91**, 5239 (1987).

[33]In Ref. 30, the bare rigidity constant $K_M(a)$ is varied by using surfactants with different chain lengths. This allows phase diagrams to be studied over a broader range of values of bare reduced rigidity $K_M(a)/T$ than could be studied by varying temperature (or our parameter z) alone. The balanced microemulsion case, considered in our paper, can be realized as in Ref. 13 by choosing the appropriate temperature for which asymmetry between oil and water disappears. In Figs. 3 and 6 of Ref. 30, this isotherm corresponds to the structure called "fish" by the authors. Moving along this line by varying ϕ_s at a 1:1 oil-to-water volume ratio is the same as moving along the constant $\hat{T}$ or constant z line of our phase diagrams in Figs. 13–18.

[34]See K.E. Bennet, H.T. Davix, and L.E. Scriven, J. Chem Phys. **86**, 3917 (1982).

[35]The continuous transition from critical end point to tricritical behavior exists in the mean-field theory of models for metamagnets which are similar to but simpler than the model considered here. See, for example, J.M. Kincaid and E.G.D. Cohen, Phys. Rep. C **22**, 57 (1975).

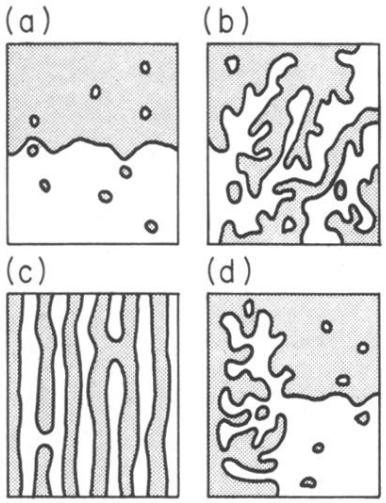

FIG. 1. (a) Dilute phases consisting of oil droplets in a water background and vice versa. The oil-rich phase is indicated with dots. Dilute phases occur at low ϕ_s (say, less than 1%) and are the analog of positive and negative magnetization ordered phases of the Ising model. (b) The random bicontinuous phase of percolating oil and water domains. This phase occurs at ϕ_s of the order of a few percent and is the analog of the paramagnetic phase of the Ising model. (c) The lamellar phase consisting of alternating layers of water and oil. This phase occurs at ϕ_s greater than a few percent. This figure shows defects in the form of water passages through an oil layer and vice versa. (d) Three-phase coexistence of the two dilute phases and the random bicontinuous phase. When there is such three-phase coexistence, the random bicontinuous phase is called the middle phase.

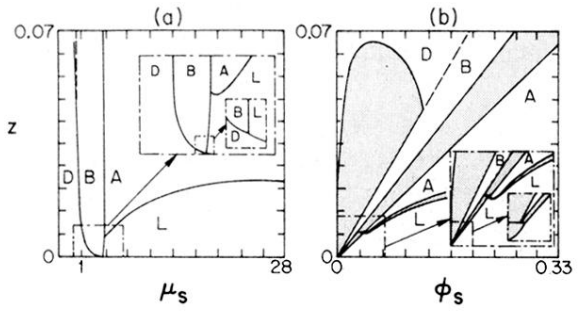

FIG. 14. (a) Type I phase diagram in the (μ_s, z) plane for $m\alpha = 2.64$ and $\mu/m = 0.38$. Insets give the regions in which two multiple points occur. (b) The same in the (ϕ_s, z) plane. In this figure and in Figs. 15–18, coexistence regions with horizontal tie lines are shaded.

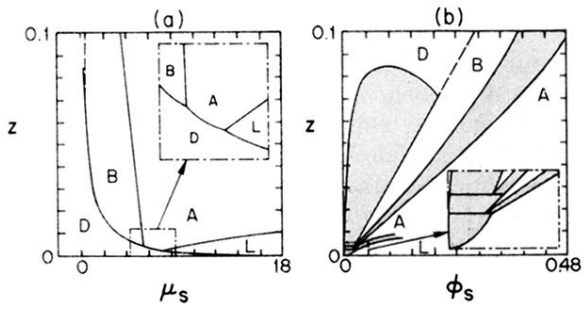

FIG. 15. (a) Type II phase diagram in the (μ_s, z) plane for $m\alpha = 2.22$ and $\mu/m = 0.34$. The inset gives the region with two triple points. (b) The same in the (ϕ_s, z) plane.

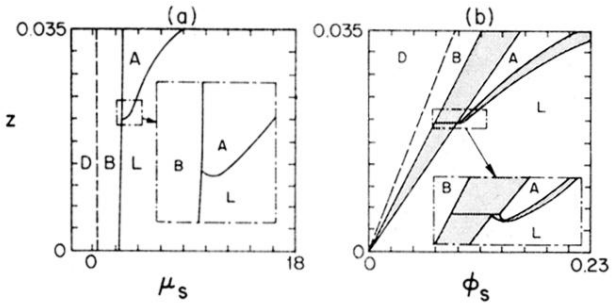

FIG. 16. (a) Type III phase diagram in the (μ_s,z) plane for $m\alpha=3.18$ and $\mu/m=043$. The inset magnifies the D-B-A triple point. (b) The same in the (ϕ_s,z) plane.

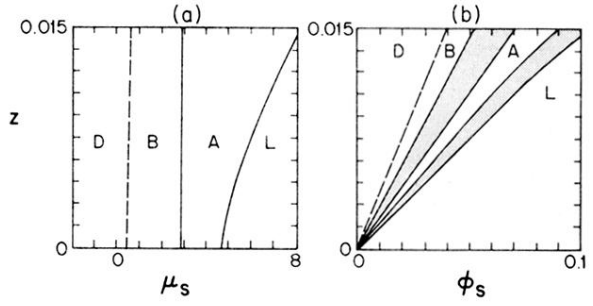

FIG. 17. (a) Type IV phase diagram in the (μ_s,z) plane for $m\alpha=3.18$ and $\mu/m=0.32$. (b) The same in the (ϕ_s,z) plane.

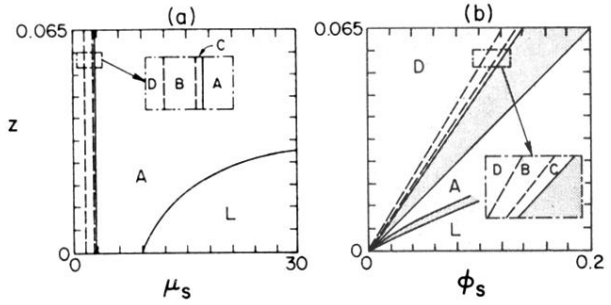

FIG. 18. (a) An example of a (μ_s, z) phase diagram containing the C phase ($m\alpha=6$, $\mu/m=0.1$). (b) The same in the (ϕ_s, z) plane.

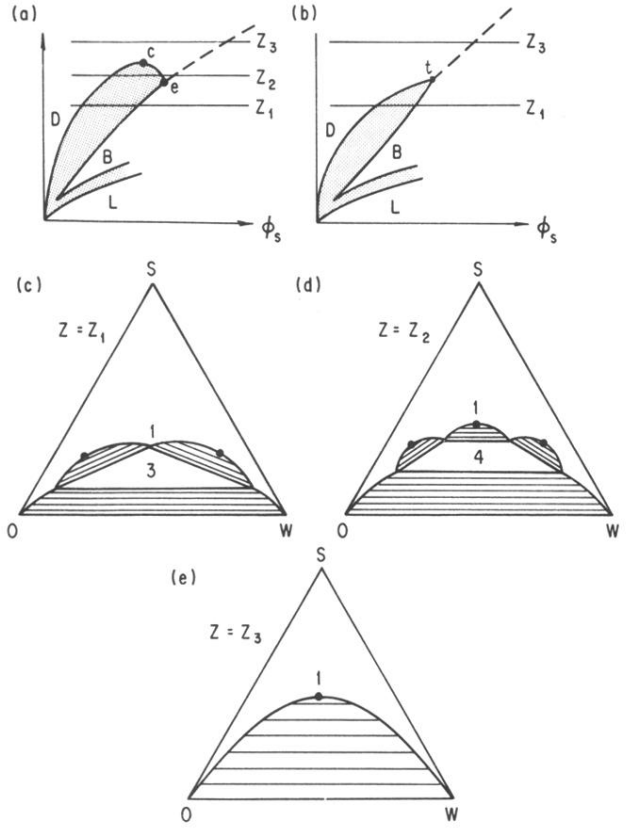

FIG. 23. (a) Schematic representation of a typical type I phase diagram of balanced microemulsion at equal volume of oil and water. It has a region of four-phase coexistence between the critical end point e and the critical point c. An alternative to (a) is the diagram shown in (b) with a tricritical point t. (c)–(e) give schematic ternary oil-water-surfactant phase diagrams corresponding to values $z = z_1$, z_2, and z_3 which are indicated in (a) and (b). For simplicity, we depict only equilibria between uniform phases. Two-phase equilibria are indicated by tie lines, while one-, three-, and four-phase regions are indicated with numbers 1, 3, and 4. Various critical points are indicated by dots.